Fuel Sensitivity Effects on Ignition, Combustion and PAH Emissions in Diesel Engine Conditions

BY

SIDDHARTH KISHOR JAIN

B.E., University of Mumbai, 2015

THESIS

Submitted as partial fulfillment of the requirements
for the degree of Master of Science in Mechanical Engineering
in the Graduate College of the
University of Illinois at Chicago, 2018
Chicago, Illinois

Defense Committee:

Dr. Suresh Aggarwal, Chair and Advisor

Dr. Kenneth Brezinsky, Mechanical and Industrial Engineering

Dr. Patrick Lynch, Mechanical and Industrial Engineering

ACKNOWLEDGEMENTS

I would like to thank my thesis advisor Dr. Suresh Aggarwal for giving me the opportunity and constant support throughout my research which helped me to achieve my research academic goals. He has trained and taught me well and opened my mind in various aspects. I would like to thank my thesis committee members Dr. Kenneth Brezinsky and Dr. Patrick Lynch for being in my thesis committee and providing me valuable feedback.

The help provided by Dr. P. K. Senecal and his colleagues at Convergent Science in running the Converge code is greatly appreciated. The authors acknowledge the Advanced Cyberinfrastructure for Education and Research (ACER) group at UIC (https://acer.uic.edu) for providing HPC resources that have contributed to the spray results reported in this paper.

I would also like acknowledge my Flow and Combustion Simulation Laboratory mates Ramachandraiah Krishna Chaitaniya Kalvakala, Abhijeet Sanjay Badhe, Rajesh Shereon, Saurabh Sharma and Hussain Kadim for making my journey so enjoyable and yet knowledgeable one. Last but not the least, I want to thank my family for their continuous support and understanding during my Master of Science degree.

Contribution of Authors

Summary of the thesis gives the insight of the study conducted. Chapter 1 is the introduction and literature review that places my thesis topic in the context of larger and related field and also highlights the significance of my research. Chapter 2 covers the computational methods used in this research work. Two tools Chemkin and Converge are used in this study and , the theory of these simulation tools are summarized based on their theory manuals (Reaction Design, CHEMKIN-PRO 15141, Reaction Design, San Diego, 2015) and (Richards KJ, Senecal PK, Pomraning E. CONVERGE (Version 2.2. 0) Manual, Convergent Science. Inc., Madison, WI. 2014). Chapter 3 covers the validation of all the computational models with experimental data. I am the main contributor to the simulation work under the guidance of my advisor, Dr. Suresh Aggarwal. Chapter 4 summarizes the results from the research work of spray ignition and partially premixed flames. And conclusion of this study is presented in chapter 5. All these chapters represent one published manuscript (Siddharth Kishor Jain and Suresh K. Aggarwal, Compositional effects on the ignition and combustion of low octane fuels under diesel conditions, *Fuel*, 2018, *220*, 654-670 DOI: 10.1016/j.fuel.2018.02.015). Chapter 4.4 discussed about the effect of fuel sensitivity on PAH in partially premixed flame, this work is anticipated to be published. For all the published manuscript and manuscript to be published in future, I am the first author. My research mentor Dr. Aggarwal played an important role in the writing of these published manuscript. And Mr. Abhijeet Sanjay Badhe also helped me in writing the manuscript for the to be published.

TABLE OF CONTENTS

LIST OF TABLES

LIST OF FIGURES

LIST OF ABBREVIATIONS

ϕ	Equivalence Ratio
A1	Benzene (C_6H_6) include symbols for A2-A5
A2	Napthalene ($C_{10}H_8$)
A3	Phenanthrene ($C_{14}H_{10}$)
A4	Pyrene ($C_{16}H_{10}$)
A5	Benzo[e]pyrene ($C_{20}H_{12}$)
LPZ	Lean premixed zone
LTC	Low temperature combustion
MON	Motor octane number
NPZ	Non-premixed zone
PAH	Polycyclic aromatic hydrocarbons
PRF	Binary primary reference fuel
RON	Research octane number
RPZ	Rich premixed zone
S	Fuel sensitivity
TPRF	Ternary primary reference fuel

SUMMARY

The amount of non-paraffinic components is directly associated with fuel sensitivity (S), which is an important consideration for using low-octane and low-cetane fuels in direct injection engines. In this research we examine the effects of S and RON (research octane number) on the ignition and combustion behavior of naphtha fuel surrogates in homogeneous mixtures and diesel sprays. Two binary blends (PRF70 and PRF80) and four ternary blends (TPRF70-a, TPRF70-b, TPRF80-a, TPRF80-b), with varying amounts of iso-octane n-heptane, and toluene, are considered. Simulations are performed using a reaction mechanism with 109 species and 543 reactions. The mechanism is validated against the shock tube and rapid compression machine ignition data, and non-reacting spray data. Ignition simulations in homogeneous mixtures are performed using CHEMKIN-Pro for a temperature range of 625-1250K, equivalence range of ϕ=0.5-2.0, and pressure of 55 bar. The study is then extended to examine the transient ignition and flame structure in liquid fuel sprays in a constant-volume combustion vessel using the CFD software CONVERGE. Results indicate that the temperature dependence of ignition characteristics in both homogeneous mixture and spray is strongly influenced by fuel sensitivity. In particular, it affects the NTC behavior and temperature dependence of the 1st and 2nd stage ignition processes. The ignition kernel structure in sprays is also strongly modified by fuel sensitivity, as the ignition kernel in ternary sprays involves rich mixtures, while that in binary sprays contains near stoichiometric mixtures, Consequently, the spray flame structure is modified by sensitivity. While the spray flame is characterized by partially premixed combustion involving a lean premixed zone (LPZ), a rich premixed zone (RPZ), and a nonpremixed zone (NPZ), the effect of sensitivity is to enhance the relative contribution of RPZ compared to those of NPZ and RPZ. In addition, due to

enhanced ignitability, the flame in ternary sprays is located closer to the injector compared to that in binary sprays. The effect of higher RON is to increase the ignition delay time. Consequently, the ignition kernel involves relatively leaner mixtures, and the flame structure is characterized by increased contributions from LPZ compared to RPZ, and flame liftoff length is increased. Increasing the initial reactor temperature has the opposite effect. A sensitivity analysis is performed to identify reactions that characterize the reduced and enhanced ignitability of ternary blends at low and high temperatures, respectively. In this work, we also examine the effects of fuel sensitivity on PAHs emissions in partially premixed counterflow flames burning one binary blend (PRF70) and two ternary blends fuel (TPRF70-a TPRF70-b). Four different mechanisms are evaluated for their predictive capabilities for PAHs emission in these flames. The mechanisms include the Park et al. reduced mechanism, CRECK mechanism, Wang et al. mechanism, and Cai and Pitsch mechanism. Counterflow flames are simulated using CHEMKIN-Pro, and these four mechanisms are evaluated by comparing their predictions of PAH species against the PAH LIF signals for fuel blends containing 10% and 20% toluene. The PAH species considered in this evaluation include A1 (benzene, C6H6), A2 (naphthalene, C10H8), A3 (phenanthrene, C14H10), A4 (pyrene, C16H10), and A5 (Benzo[e]pyrene, C20H12) depending upon the mechanism. Park et al. mechanism was found to mimic the trend of increase in PAH with increase of iso-octane in the fuel. For all three fuels, the global flame structures are found to be similar, characterized by a rich premixed zone (RPZ) on the fuel side and a non-premixed zone (NPZ) on the oxidizer side. Most of PAHs are formed near RPZ. The fuel with high sensitivity shows higher PAHs emission, which is due to the presence of toluene (C6H5CH3) that increases the production of benzene (A1), an important precursor for the formation of larger PAHs. The

detailed path and sensitivity analysis were carried out to identify the dominant reactions for the formation of A1 and A4 (pyrene). Toluene reacting with hydrogen (H) is observed to be the dominant reaction for the formation A1, while benzyl radical (C6H5CH2) reacting with indenyl radical (C9H7) is the dominant reaction for the formation of A4 in ternary blends. In addition, the effects of equivalence ratio (level of fuel-air premixing) and low temperature combustion (achieved by using N2 dilution of the fuel stream) on PAH emissions are discussed.

1. INTRODUCTION

1.1 Motivation

(Previously published as Siddharth Kishor Jain and Suresh K. Aggarwal, Compositional effects on the ignition and combustion of low octane fuels under diesel conditions, *Fuel*, 2018, *220*, 654-670 DOI: 10.1016/j.fuel.2018.02.015)

The transportation sector is still mainly dependent on petroleum-based fuels, which provide about 95% of the energy [1]. Compression ignition (CI) engines are 20-30% more efficient than spark-ignited (SI) gasoline engines, but gasoline engines have advantages of low emissions over diesel. Challenges of NOx and particulate matter (PM) remain with diesel combustion. Hence, different approaches have been investigated to exploit the advantages of both CI and SI engines in order to achieve SI engine like emissions with CI engine like efficiencies. Low temperature combustion (LTC) is one of such approaches, which can achieve low emissions with high thermal efficiencies. There are various advanced combustion engine (ACE) designs that rely on LTC, namely homogeneous charge compression ignition (HCCI), gasoline direct injection compression ignition (GDICI), premixed charge compression ignition (PPCI) and their variants [2]. Kalghatgi et al. [3] introduced the concept of improved HCCI using high-octane fuels by direct injection into a CI engine. Since LTC is achieved by controlled ignition, fuel properties like cetane number (CN) and fuel volatility are important aspects to achieve LTC. There are still many challenges to achieve LTC in compression-ignition engines, especially in HCCI mode due to small range of operating conditions. This is due to a lack of control of ignition timing, which makes combustion phasing difficult resulting in low power densities. As reported in previous studies [3,

4], autoignition is the primary mode of control for implementing the LTC, and accurate depiction of ignition kinetics is important for developing reliable simulation models for ACE.

Recent studies [5, 6] have shown that the fuels with low cetane number can achieve premixed LTC with satisfactory control of combustion phasing in diesel engines. This is due to their longer ignition delay time, which allows more advanced injection providing sufficient time to get adequately mixed mixture, and combined with optimum EGR, could provide high power densities with reduced engine out emissions. Fuels with research octane number (RON) between 50-70, such as naphtha fuel, are considered good candidate for ACE to achieve LTC [7]. Naphtha is one of the first product during the distillation of crude oil, hence is cost effective. Cung et al. [8] conducted a sensitivity analysis to examine the effects of various parameters on ignition in partially premixed combustion (PPC) mode. They found that compared to injection pressure, the intake pressure and air/fuel ratio more strongly affect the ignition, combustion and emissions behavior. Yang et al. [9] observed NOx reduction and efficiency improvement in single cylinder diesel engine operating on premixed compression ignition concept using straight run naphtha fuel with RON≈58.8. Low octane fuels like naphtha fuel are useful for such LTC operations due to their long ignition delay which gives sufficient fuel-air mixing and thus facilitates ignition near stoichiometric conditions. Zhang et al. [10] observed that naphtha fuels with RON of 59 and 69 used in CI engine could achieve enhanced premixed combustion, which is beneficial for reduction in soot emissions. However accurate modelling of ignition chemistry is required for the use of naphtha fuel in LTC engines, since autoignition is the primary control mechanism for optimizing the engine performance. Moreover, a good surrogate needs to be formulated for naphtha fuel which can mimic its physical as well as the chemical properties and represent accurate

atomization and ignition characteristic of this fuel. Primary reference fuels (PRFs) with the appropriate mixtures of heptane and iso-octane, have been commonly used as surrogates for octane fuels [11]. However, as discussed in previous studies [12, 13, 14], since a PRF is only composed of paraffinic components, its sensitivity (S), defined as the difference between RON (Research Octane number) and MON (Research Octane number) is zero. Fuel sensitivity is a measure of non-paraffinic content, such as aromatics, in the fuel, and fuels with high sensitivity exhibit different temperature dependency at low, medium and high temperatures [13, 14]. Such fuels show high reactivity at high temperatures and low reactivity at low temperatures, as well as exhibit different degree of negative temperature coefficient (NTC) behavior. Consequently, PRFs are not a good candidate for the surrogate fuel to mimic ignition, combustion and emission characteristics of gasoline and naphtha fuel in CI engine. Therefore, a more complex surrogate with three or more components is needed to represent the reactivity of high sensitivity fuels over a range of diesel engine conditions.

Various studies have examined the effect of toluene addition to PRF surrogates to account for the effect of fuel sensitivity (S), and to evaluate its capabilities to mimic the behavior of high sensitivity fuels like gasoline [15, 16, 17, 18]. Gauthier et al. [18] compared gasoline RD387 with its ternary primary reference fuel (TPRF) surrogate (63% iso-octane, 20% toluene, 17% n-heptane by volume) to study auto-ignition in shock-tube setup and observed that ternary surrogate accurately mimic the auto-ignition of gasoline at high temperatures (T > 850K). Chaos et al. [17] observed that addition of toluene in PRF, i.e., three-component surrogate (PRF + toluene) for gasoline reduces the NTC behavior of the surrogate. To get an accurate surrogate to mimic the ignition characteristic of a fuel, the surrogate should be properly formulated to match the RON

of the desired fuel. To this end, Kalghatgi et al. [12] formulated a correlation to calculate the composition of iso-octane, n-heptane and toluene to match the RON and S of the desired fuel. Javed et al. [13] developed three-component surrogates to match the RON and MON of two-octane and two low-octane naphtha fuels, in order to study the ignition characteristics of these fuels in shock-tube (ST) and rapid compression machine. It was observed that three-component fuels formulated using Kalghatgi [12] show strong dependency on fuel sensitivity in the NTC region. Javed et al. [14] showed that simulations using a multicomponent fuel provide better agreement with the measured ignition behavior of light naphtha (RON~64.5) in ST and RCM experiments. Singh et al. [19] examined ignition behavior of various surrogates including PRFs and TPRFs under homogeneous conditions to characterize the effects of fuel composition on RON and fuel sensitivity. It was observed that fuel with high sensitivity (S) show longer first stage ignition delay and shorter second stage ignition delay. Also fuels with olefins showed smaller low temperature heat release (LTHR) but lacked NTC behavior i.e. these fuels are more reactive at intermediate temperatures. Szybist et al. [20] used three fuels with fuel sensitivity S = 0, 6.5 and 12, but nearly the same RON (99.2-100), and performed experiments in single cylinder, direct injection engine. They observed that at high loads the knock resistance becomes proportional to S, while at low load knock resistance is inversely proportional to S, with fuel with S = 12 being the most knock resistant. This is due to the dependence of ignition delay on load and S. Moreover, the use of multicomponent surrogates is not only important to mimic the ignition and combustion characteristics but also the emission behavior of real fuels. Since the fuel sensitivity provides a measure for the amount of aromatic component in the fuel, the fuel sooting characteristics can be expected to be strongly influenced by fuel sensitivity [21, 22]. Park et al.

[21] examined the effect of amount of toluene and iso-octane in the fuel on PAH emissions in nitrogen diluted gasoline opposed-jet flames. They observed that PAH emission increases with the amounts of toluene and iso-octane in the fuel. An et al. [22] studied the effect of toluene content in the fuel on PAH emissions in different combustion modes like partially premixed combustion and homogeneous charge compression ignition (HCCI). In both the modes, the PAH emissions were increased with the increase in toluene content of the fuel. Thus, it is important to characterize the effect of fuel sensitivity not only on ignition and combustion characteristics but also on emission characteristic under diesel engine conditions.

1.2 **Objectives**

The objective of this study is to identify the effect of fuel sensitivity on ignition and combustion, and PAH emission characteristics under diesel engine conditions. The eventual goal is to formulate a surrogate to mimic the combustion and emission behavior of real fuels accurately.

1.2.1 Ignition Study of Homogeneous Mixtures and Fuel Sprays

(Previously published as Siddharth Kishor Jain and Suresh K. Aggarwal, Compositional effects on the ignition and combustion of low octane fuels under diesel conditions, *Fuel*, 2018, *220*, 654-670 DOI: 10.1016/j.fuel.2018.02.015)

The computational study is carried out on the ignition and combustion behavior of two binary blends and two ternary blends in homogeneous mixtures and fuel sprays. The major objective is to characterize the effects of fuel reactivity (RON) and fuel sensitivity (S) on the

transient ignition and flame development under diesel engine conditions. The two binary blends used in this study are PRF70 and PRF80, with the corresponding ternary blends being TPRF70-a and TPRF80-a. The ternary blends with different RON and fuel sensitivity are adopted from ref. [13]. These blends have different amounts of n-heptane, iso-octane and toluene. The physical properties of n-heptane, iso-octane and toluene at 293K and 1 atm are listed in Table 1. Two additional blends used in this study with higher fuel sensitivity are TPRF70-b and TPRF80-b, which are formulated using the correlation from ref. [12] to match the RON with increased fuel sensitivity.

TABLE 1: Relevant physical properties of iso-octane, n-heptane and toluene at 293K and 1 atm.

	Iso-Octane	n-Heptane	Toluene
Critical Temperature (°C)	544	540	592
Boiling Temperature (°C)	99	98.3	111
Density (kg/m3)	692	684	867
Vapor Pressure (kPa)	4.5	4.7	2.3
Liquid Viscosity (mPa-s)	0.528	0.431	0.611
Heat of vaporization (KJ/kg)	309	365	414
Specific Heat (KJ/kg-K)	2.05	2.24	1.68
Surface Tension (N/m)	0.019	0.021	0.029

The compositions of these blends in volume percentage with their RON, MON, and fuel sensitivity are provided in Table 2. The kinetic model used for ignition and combustion study is that of Wang et al. [23], which involves 109 species and 543 reactions, and includes chemistry for the formation of NOx and PAH (A1 - Benzene, A2 - Naphthalene, A3 – Phenanthrene, A4 - Pyrene) species. The mechanism has been previously validated against ignition delays, laminar flame speeds and species profiles in premixed flames. Additional validation is provided here using the ST and RCM ignition delay data from [13]. The mechanism is also compared with the predictions of LLNL mechanism [24] with 679 species and 3479 reactions. Simulations for homogeneous mixture are performed using CHEMKIN Pro [25] tool to examine the effect of fuel reactivity and sensitivity on ignition characteristics, especially in NTC region.

TABLE 2: PRF and TPRF surrogates investigated in this work.

Surrogate	iso-Octane	n-Heptane	Toluene	RON	MON	Sensitivity (S)
PRF70	70%	30%	0%	70	70	0
PRF80	80%	20%	0%	80	80	0
TPRF70-a	42.8%	36.23%	21.29%	70[a]	66[a]	4
TPRF70-b	28%	40%	32%	70.05[b]	64.4[b]	5.7
TPRF80-a	39.85%	28.58%	31.57%	80[a]	74.3[a]	5.7
TPRF80-b	30%	30.95%	39.05%	80[b]	73.2[b]	6.8

a RON and MON estimated by Javed et al. [13].

b RON and MON estimated using correlations developed by Kalghatgi et al. [12]

c Sensitivity S=RON – MON (estimate).

Simulations are then performed for 3-D reacting sprays in Sandia constant volume reactor [26] to examine the effect of RON and S on the transient ignition and flame development using the 3-D CFD tool CONVERGE [27].

1.2.2 Counterflow Partially Premixed Flames

The thesis also includes a computational study on the combustion and soot characteristics of one binary and two ternary blends (PRF70, TPRF70-a and TPRF80-a). The main objective is to study the effect of fuel sensitivity (S) on PAHs emission in partially premixed counterflow flames. The computational study employs the CHEMKIN Pro software [25] as mentioned earlier. The kinetic mechanism used for this purpose is developed by Park et al. [21], it involves 574 species and 3379 reactions including the PAH formation mechanism. This mechanism is validated with species profile in counterflow diffusion flames. The PAH study was carried in partially premixed flames in counterflow jet configuration due to its simple flow field and its relevance to diesel engine combustion [28]. The reaction path and sensitivity analysis are also performed to identify major paths and reactions for the formation of benzene (A1) and pyrene (A4) in these flames.

2. Computational Model

(Previously published as Siddharth Kishor Jain and Suresh K. Aggarwal, Compositional effects on the ignition and combustion of low octane fuels under diesel conditions, *Fuel*, 2018, *220*, 654-670 DOI: 10.1016/j.fuel.2018.02.015)

Simulations for ignition in homogeneous mixtures under constant volume conditions were performed using the CHEMKIN-PRO software [25]. Subsequently, the transient spray ignition and flame simulations were performed using the CONVEGRE software [27], which is a general-purpose code for 3-D non-reacting and reacting spray computations. The computations are based on a Eulerian-Lagrangian formulation. The gas-phase flow field in this study is defined by the Favre Averaged Navier Stokes equations including RNG turbulence model [29]. In this study the liquid droplets are represented by discrete number of parcels, which are tracked using a Lagrangian method. The spray simulations include models for fuel atomization, vaporization, droplet breakup, collision and coalescence, spray-wall interaction. Detailed description of these is reported in the CONVERGE manual and related articles [27, 30]. Blob injection method is used to simulate spray droplet parcels with the diameter equal to nozzle diameter [31]. The breakup process of liquid droplet parcels is simulated using Kelvin–Helmholtz and Rayleigh–Taylor models [32], while the droplet collisions are modeled using the No Time Counter (NTC) algorithm [33]. A dynamic droplet drag model [34] is used, in which the drag coefficient is calculated by considering the variation in the drop shape from sphere to disk. A multicomponent vaporization model is used to model droplet evaporation for all the six fuel blends [35].

The fuel ignition and combustion chemistry is modeled by incorporating the Wang et al. mechanism [23] in the SAGE chemical kinetic solver. In contrast, the well mixed models have shown the precise predictions for the two-phase flow spray and combustion characteristics [36]. Recent studies have provided additional validation for such models for both gasoline and CI engines [37]. The computational domain used in this study has a cubical geometry with sides of 108 mm x 60 mm x 60 mm. This domain represents the Sandia contact volume reactor [37] in order to achieve diesel engine conditions for the simulation. In CONVERGE the grid generation is performed during the runtime with the capability of fixed embedding, i.e., permanent high resolution of grid over the base cell size in the regions with fixed high gradients, such as near the injector, as well as adaptive mesh refinement (AMR) based on the gradients of temperature, velocity and OH species. The expression adopted in Converge [27] to define grid scaling and fixed embedding is

$$scaled\ grid, dx\_embed = \frac{dx\_base}{2^{grid\_scale,\ embed\_scale}} \quad \text{.... (1)}$$

where grid_scale and embed_scale are the scaling factors, and scale grid and dx_embed are the new base grids. The base grid size is 2 mm and the minimum grid near the injector region was set to 0.125 mm, and 4 levels of AMR for temperature, velocity and OH species. The sliced view of the computational domain and the generated mesh at 2ms are shown in Fig. 1. The simulation results for grid independence and validation of the reaction mechanism and spray models are presented in the next section.

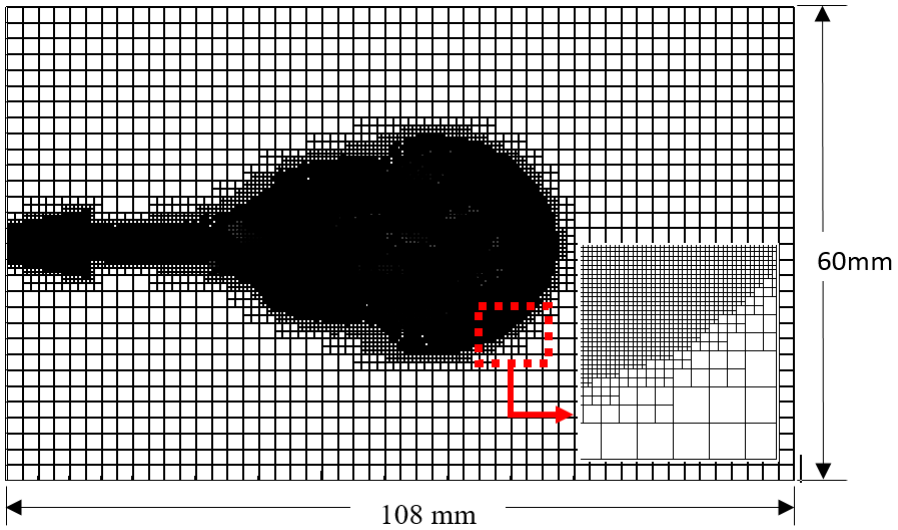

Fig. 1. Grid generated in CONVERGE at 2 ms. At this time there is a developed flame for PRF70 spray. The field of view is 108 mm x 60 mm.

The correlation used to formulate the fuel sensitivity of blends used in this study with specific research octane rating is developed by Kalghatgi et al. [12] and is given by

$$TMF = \frac{V_t}{V_t + 0.643V_i + 0.72515V_n} \quad \text{.... (2)}$$

Here TMF is the toluene mole fraction, V_t is the volume fraction of toluene in the blend, V_i is the volume fraction of iso-octane and V_n of n-heptane in the blend. In calculating the TMF the density (g/cc)/molecule weight used for toluene, n-heptane and iso-octane are 0.867/92.1, 0.684/100.2 and 0.692/114.2 respectively. PRF in equation below is the octane number of the PRF without toluene,

$$\frac{PRF}{100} = \frac{V_i}{V_i + V_n} \quad \text{.... (3)}$$

Since PRF blends only consist of n-heptane and iso-octane. And as we know,

$$V_i + V_n + V_t = 100 \quad \text{.... (4)}$$

Now research octane number (RON) of the fuel is calculated using the correlation below,

$$RON = aTMF + b \quad \text{.... (5)}$$

Where,

$$a = 118.09 + 1.0355PRF \quad \text{.... (6)}$$

$$b = 1.0023PRF - 1.7774 \quad \text{.... (7)}$$

Once RON is calculated fuel sensitivity is calculated by,

$$S = 14.07TMF \quad \text{.... (8)}$$

MON can be calculated from RON and S using the Eqn.

$$S = RON - MON \quad \text{.... (9)}$$

A sensitivity analysis was performed to identify specific reactions affecting the relative ignitability and the predicted PAH levels for binary and ternary blends at different temperatures. To study the effect of S on ignition, sensitivity analysis was carried out with respect to ignition delay. In this method sensitivity coefficient is calculated by correlation,

$$S_c = \frac{t_{ign}(2A) - t_{ign}(A)}{t_{ign}(A)} \times 100 \quad \text{.... (10)}$$

Here Sc is the sensitivity coefficient, tign is ignition delay time and A is the reaction rate. First, the important reactions responsible for the production and consumption of OH were analyzed, since ignition is characterized by the sudden rise in OH concentration. For this, CHEMKIN-Pro was used to identify important reactions with the highest rate of production and consumption of OH. For this first the simulation for ignition delay is run with the homogeneous reactor option. While postprocessing the output, CHEMKIN-Pro has an option to postprocess the

rate of production of each species in the chemical kinetic mechanism. For this, the ROP option for OH was selected, which yielded the ROP (rate of production) of OH through all the reactions. Then the top 10 reactions with maximum rates of production and consumption were selected. Then the reaction rates of these reactions were doubled one by one and the ignition delay was calculated for each case to get the value of tign(2A) for each reaction. Ignition is defined by the 400K temperature increase from initial. Then the sensitivity coefficient (Sc) was calculated for each of these reactions. The sensitivity analysis to study the effect of S on PAH emissions was done with a similar method. But instead of calculating ignition delay (tign), mole fractions of A1 (benzene) and A4 (pyrene) were calculated.

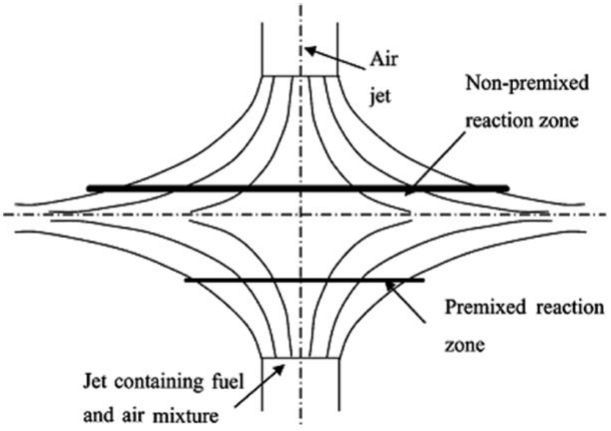

Fig. 2: A schematic of the counterflow jet configuration for partially premixed flame.

A schematic diagram of opposed jet flame configuration from Fu et al. [46] employed in this study is shown in Fig. 2. It consists of two opposing jets from two coaxial nozzles, which are separated by distance of 0.8 cm. Partially premixed flames with NPZ and RPZ were established by having a fuel rich stream from one nozzle and an oxidizer stream from another nozzle. Fuel stream temperature is 423K, since fuel is considered in vaporized form and oxidizer stream temperature is 298K, and the pressure as 1 atm. PPFs with one binary (PRF70) and two ternary

(TPRF70-a and TPRF70-b) blends are established by independently varying ϕ. The flow velocities at the nozzle exits for both the fuel and oxidizer streams are maintained at 20 cm/s for all the blends. Simulations are performed using OPPDIF in CHEMKIN-Pro.

3. Validation and Discussion

In this chapter we discuss the validation of both numerical spray model and different mechanisms used in this study with the experimental data of ignition delays, species profiles and spray penetration.

3.1 **Spray model validation**

(Previously published as Siddharth Kishor Jain and Suresh K. Aggarwal, Compositional effects on the ignition and combustion of low octane fuels under diesel conditions, *Fuel*, 2018, *220*, 654-670 DOI: 10.1016/j.fuel.2018.02.015)

Here we present the validation of the spray model used for the 3-D spray ignition simulation study. The validation is done for the simulation of non-reacting n-heptane spray, with the spray penetration ECN experimental data [26]. In order to accurately predict the ignition delay and the combustion property, it is important to validate the non-reacting spray to mimic accurate process of spray development, atomization and vaporization. The experimental condition used to simulate the non-reacting spray is given in Table 3. These conditions are based on the experimental data from ECN [26].

TABLE 3: Experimental and simulation conditions.

	Non-reacting	Reacting
Temperature [K]	1000	1000
Ambient Pressure [MPa]	4.33	5.50
O2 volume fraction [%]	0	21
Injection Pressure [MPa]	150	150
Injection duration [ms]	6.8	6.8
Injection mass [mg]	17.8	17.8
Nozzle diameter [mm]	0.1	0.1
Discharge coefficient (Cd)	0.8	0.8
Area contraction coefficient (Ca)	0.86	0.86

Figure 3 presents the simulated and measured liquid and vapor penetrations with respect to time. The simulation is done with different grid sizes, i.e. four different combinations of fixed embedding and AMR. The liquid penetration is defined as the axial distance encompassing 97% of injected liquid mass, while the vapor penetration length is based on the fuel vapor mass fraction level 1%. As shown in figure 3, before 3ms approximately i.e. initial liquid penetration, the simulated liquid and vapor penetration show good agreement with the measured data. In all the simulations done using Converge the base grid size is constant at 2mm, with fixed embedding near injector region to achieve the minimum grid size of 0.125mm and 0.25mm to constantly resolve the flow near injector accurately. And AMR is employed in with minimum grid sizes of 0.125 and 0.25 in whole computational domain. To validate different combination

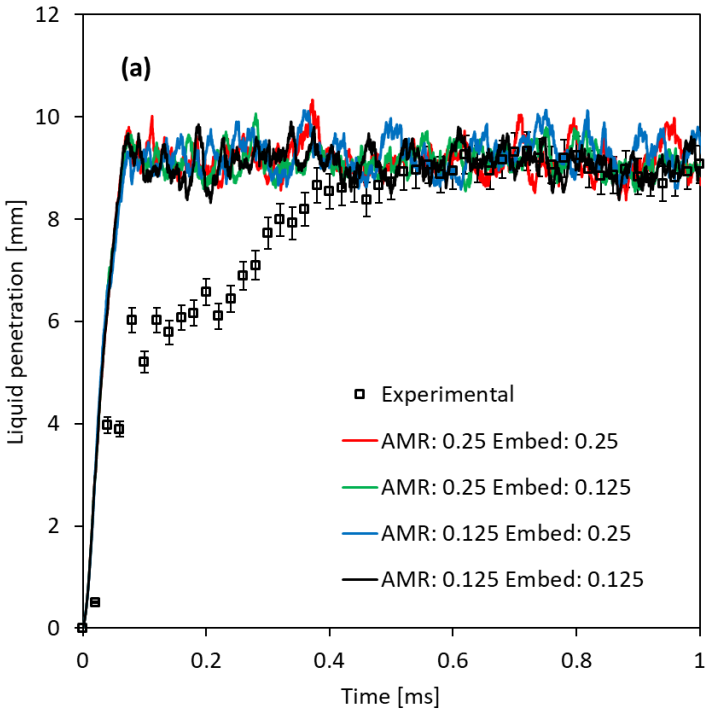

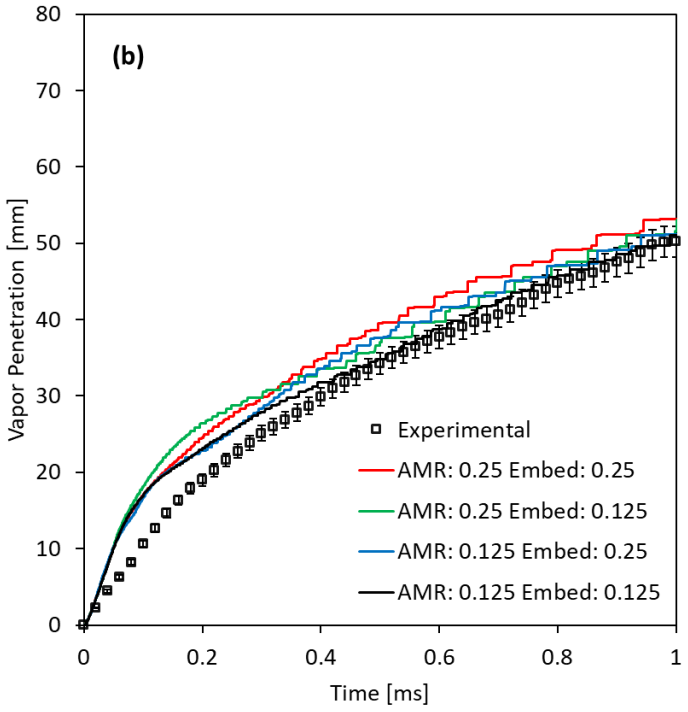

Figure 3: Measured [26] and predicted liquid (a) and (b) vapor penetrations for non-reacting n-heptane spray. Error of 4% for liquid and vapor penetration experimental data.

of fixed embedding and AMR is used to get the grid independent model. Figure 3a presents that all combinations of grid sizes give similar liquid penetrations. But in figure 3b that the fixed embedding with grid size of 0.125mm and AMR with minimum grid size of 0.125mm gives better predictions. However, there are some discrepancies between the simulated and

measure data during initial injection. As discussed by Som et al. [38] and Fu and Aggarwal [39], these discrepancies may be due to many different factors, like uncertainties in the measurement of near-nozzle flow, under-resolved flow in the near nozzle region and insufficiencies to capture the effect of nozzle inner flow.

3.2 **Ignition delay validation**

(Previously published as Siddharth Kishor Jain and Suresh K. Aggarwal, Compositional effects on the ignition and combustion of low octane fuels under diesel conditions, *Fuel*, 2018, *220*, 654-670 DOI: 10.1016/j.fuel.2018.02.015)

Mechanisms developed by Wang et al. [23] and LLNL mechanism [24] are validated with the ignition delay data of binary and ternary blends from shock-tube (ST) and rapid compression machine (RCM) experiments [13, 40]. Simulations were carried out in constant-volume, homogeneous combustion reactor using CHEMKIN-Pro software. Figure 4 presents the validation of both the mechanisms with the measured ignition delay of binary blends reported by Fieweger et al. [40]. Figure 4 presents the predicted and measured ignition delays of three different PRF blends. Both the mechanisms show fairly good agreement with the measured data, with Wang et al. mechanism slightly underpredicting and the LLNL mechanism overpredicting ignition delays.

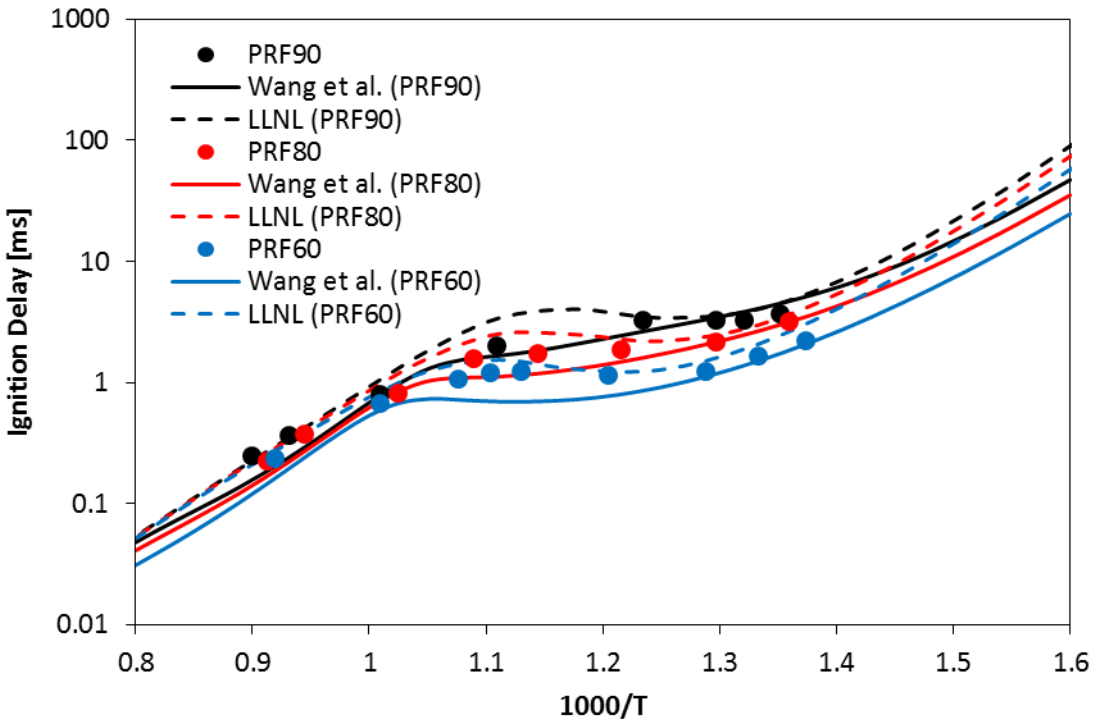

Fig. 4: Measured [40] and predicted ignition delays for three different PRF blends at P=40 bar and ϕ=1.

Figures 5 and 6 present the validation for ternary blends (TPRF70 and TPRF80 respectivley), at p = 20 bar and 40 bar and equivalence ratio of ϕ=0.5 and 1.0. The predicted data is compared with measured data reported by Javed et al. [13], which include ST data for T>800K and RCM data for T<800K. Both the mechanisms are in fairly good agreement with the experimental data for the range of pressure and equivalence ratio, with the Wang et al. mechanism underpredicting and the LLNL mechanism overpredicting ignition delays. Moreover, both the mechanisms are able to reproduce the experimentally observed NTC regime, which is relevant for CI engine. Since Wang et al. mechanism is a reduced mechanism with 109 species and 543 reactions only, this mechanism was used to carry out a detailed ignition study.

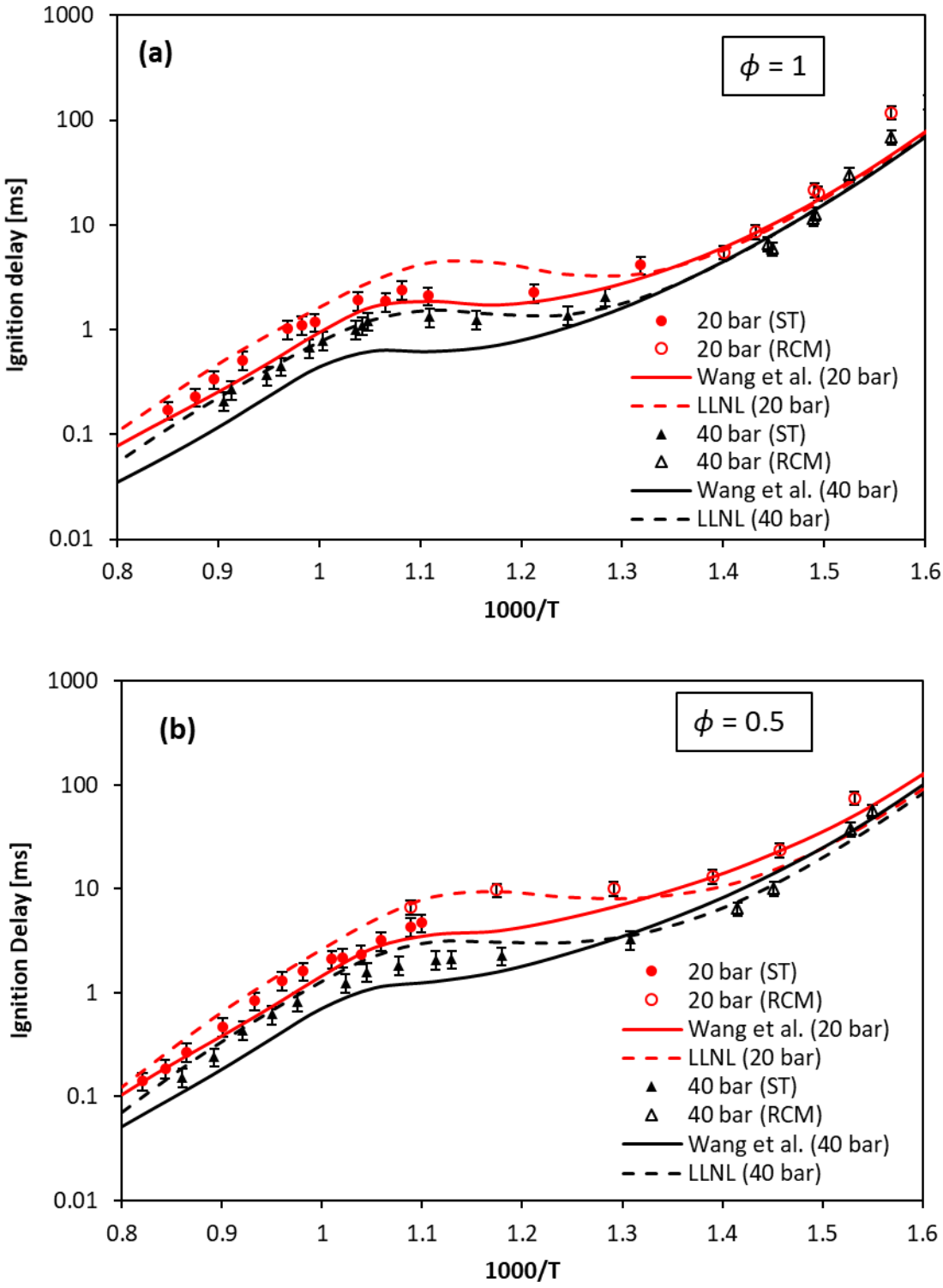

Fig. 5: Measured [13] and predicted ignition delays for TPRF70 at different P and ϕ=1.0 (a) and ϕ=0.5 (b). Error of 20% for ST and 15% for RCM experimental data.

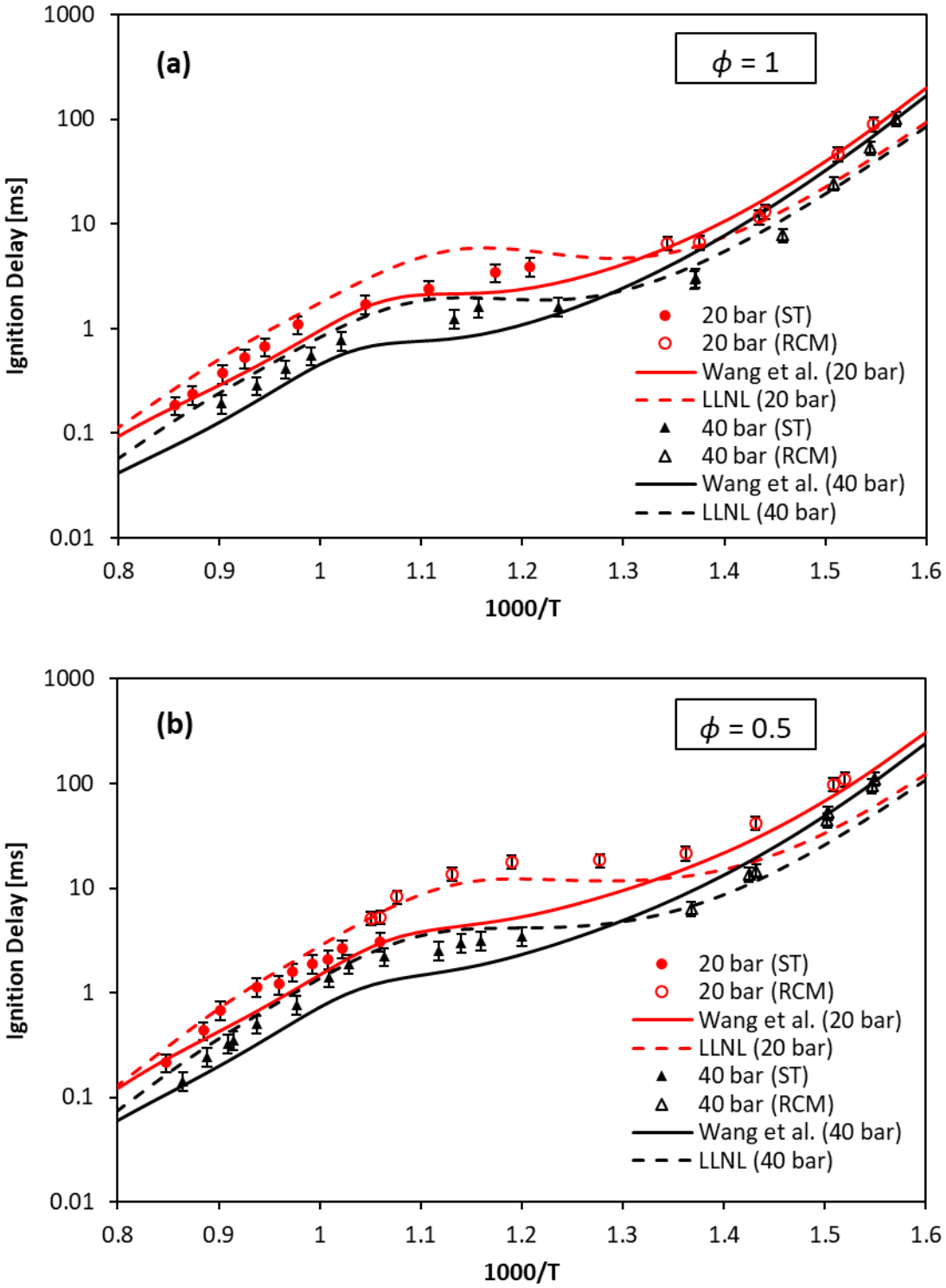

Fig. 6: Measured [13] and predicted ignition delays for TPRF80 at different P and ϕ=1 (a) and ϕ=0.5 (b). Error of 20% for ST and 15% for RCM experimental data.

3.3 **Validation of reaction mechanisms for PAH predictions**

Many comprehensive and reduced mechanisms are available for TPRF mixtures, including the mechanism for the formation PAH species up to A4 (pyrene) – soot precursor. Four mechanisms are evaluated in terms of their predictions of PAH species by using measurements of Park et al. [21] in counterflow diffusion flames. Park et al. [21] examined the effect of composition of ternary blends on PAH emissions and soot formation in counterflow diffusion flames. They used laser-induced fluorescence technique for measurements of PAHs concentrations. They also proposed a mechanism for gasoline surrogate mixtures and validated it for ignition delays, laminar premixed flame speeds and for the combustion of binary and ternary blends in counterflow diffusion flame. In these experiments, the toluene volume fraction was kept constant, while the iso-octane ratio (Ri), ratio of iso-octane to n-heptane in the ternary blends is varied from zero to unity.

Figure 7 presents the normalized maximum LIF signals and the predicted peak mole fractions of PAHs (A2–A5) for T10PRF and T20PRF, which contain. 10% and 20% toluene, respectively. LIF signals with higher wavelength (>400Nm) are considered to represent the larger PAH molecules like A4 and A5, while lower wavelength corresponds to smaller PAH like A2 and A3. In this validation A1 is not considered since the minimum wavelength used for LIF signal is high, which makes it difficult to detect A1. However, it should be noted that it is incorrect to associate a discrete wavelength with any one PAH species owing to complex and broadband absorption/emission spectra of PAH species. As shown in Figure 7 the predicted PAH species profiles show the same trend as that exhibited by the LIF signal for the effect of increasing the amount of iso-octane in the blend. In T10PRF flame the concentration of PAH increases with the

increase of iso-octane in the fuel, and the same trend is seen in the LIF signal. LIF signals with shorter wavelength (330 nm, 400 nm) increase linearly similar to smaller PAHs (A2, A3), while LIF signals at large wavelength (>400Nm), increase non-linearly, similar to larger PAHs (A4, A5). This shows good agreement between the predicted PAHs and the measured data. Similar conclusion can be drawn for T20PRF.

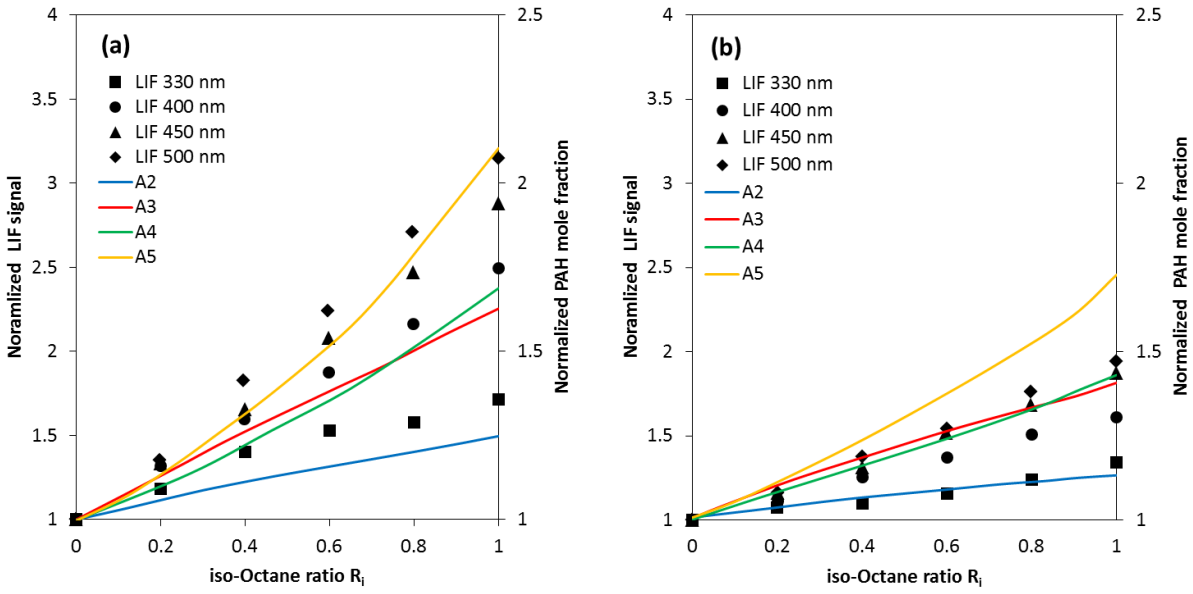

Fig. 7: Measured normalized maximum LIF signals and computed PAHs for (a) T10PRF and (b) T20PRF blends using the Park et al. mechanism.

Three other mechanisms validated in this section are the Wang et al. mechanism [23], Cai and Pitsch mechanism [41] and Creck mechanism [42]. All these mechanisms are developed for gasoline surrogate fuels like TPRF and also include PAH chemistry. They were used for the same set of diffusion flames burning T10PRF and T20PRF fuels, as discussed above. Figure 8 shows the comparison of predicted PAH species by using the Creck mechanism and measured LIF signal. The Creck mechanism includes reactions for A1 to A4 species only. This mechanism shows a fairly good agreement with the experimental data, including the increase in PAH concentration with

the increase of iso-octane in the blend. But it has limitation in accurately predicting the rate of increase of PAH concentrations, as it fails to predict the linear increase of A4 and A5.

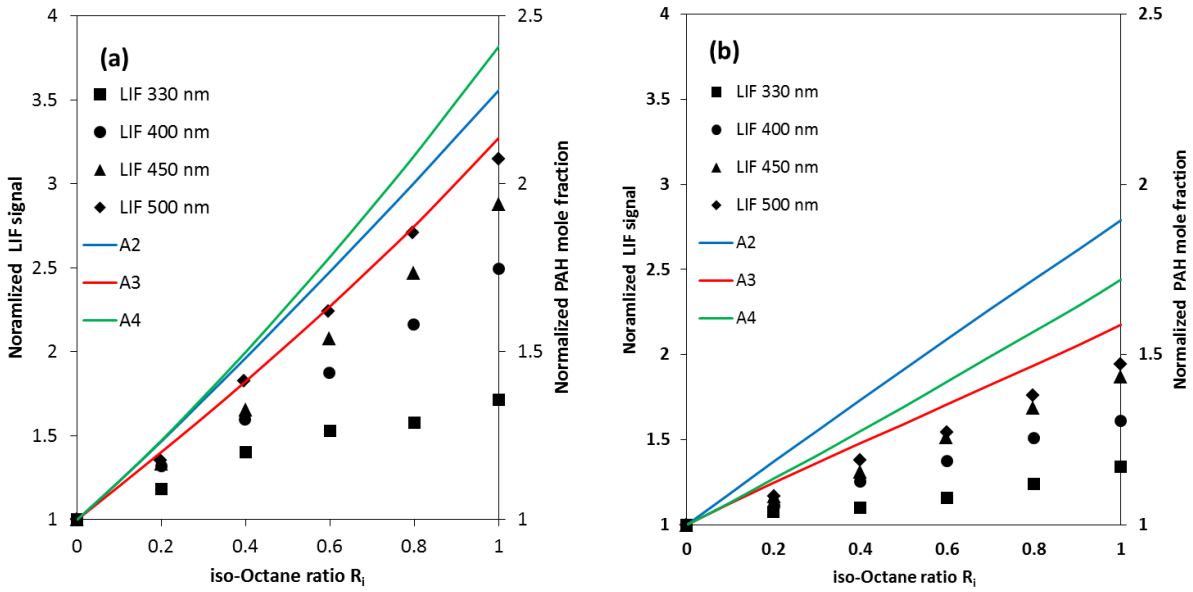

Fig. 8: Measured normalized maximum LIF signals and computed PAHs for (a) T10PRF and (b) T20PRF blends using the CRECK mechanism.

Figures 9 and 10 present the comparison of PAH predictions using the Wang et al. [23] and Cai and Pitsch mechanisms [41] with the measured LIF signals. Both these mechanisms incorporate reactions for A1 to A4. Although the Wang et al. mechanism showed good predictions of ignition and combustion in previous study for spray flames, it has limitation to predict the PAH species accurately in counterflow diffusion flame. Both the Wang et al. and Cai and Pitsch mechanisms are unable to mimic the trend of increase of PAH species with the increase of iso-octane in the fuel.

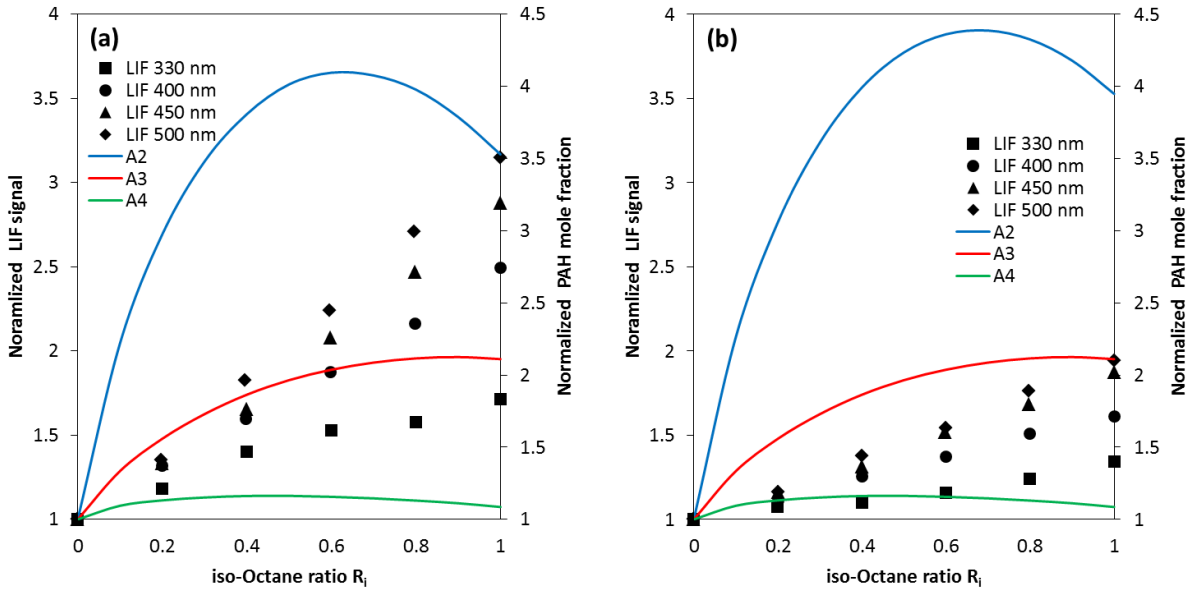

Fig. 9: Measured normalized maximum LIF signals and computed PAHs for (a) T10PRF and (b) T20PRF blends using the Wang et al. mechanism.

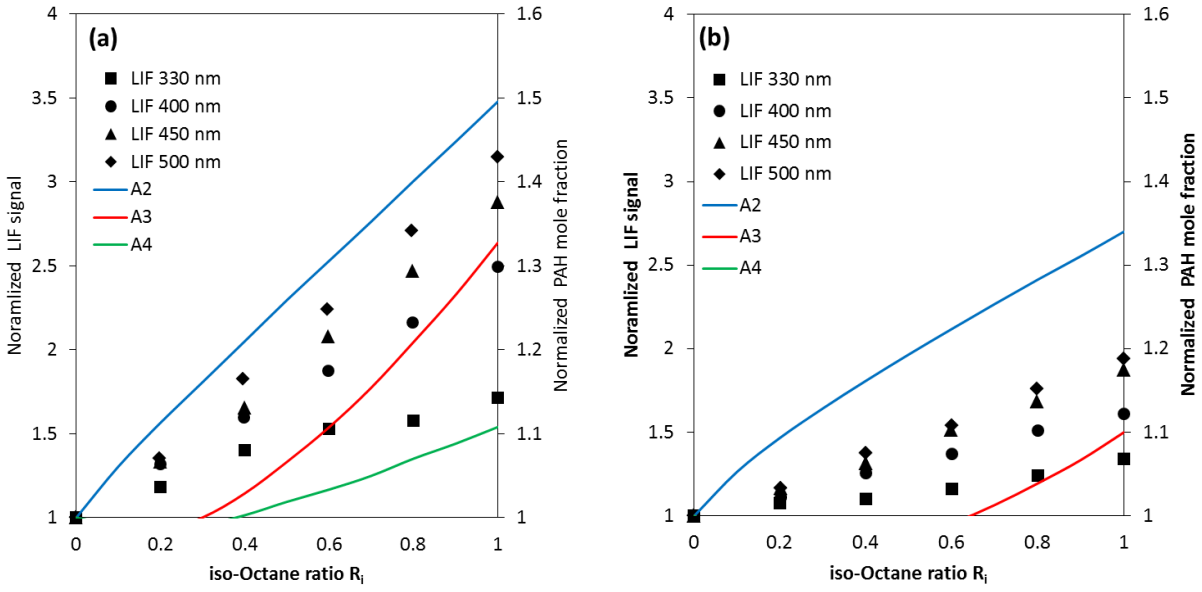

Fig. 10: Measured normalized maximum LIF signals and computed PAHs for (a) T10PRF and (b) T20PRF blends using the Cai and Pitsch mechanism.

4. Results and Discussion

In this chapter we discuss the effect of fuel sensitivity on the ignition of homogeneous mixtures, and ignition and flame evolution in fuel sprays. In addition, results are presented concerning the effect of fuel sensitivity on PAH emissions in partially premixed counterflow flames.

4.1 **Ignition of Fuel-Air Homogeneous Mixture**

(Previously published as Siddharth Kishor Jain and Suresh K. Aggarwal, Compositional effects on the ignition and combustion of low octane fuels under diesel conditions, *Fuel*, 2018, *220*, 654-670 DOI: 10.1016/j.fuel.2018.02.015)

Here we discuss the effect of fuel sensitivity (S) on the ignition of binary and ternary blends under homogeneous conditions at different initial temperatures. Simulations are performed in Constant volume reactor using CHEMKIN Pro simulation tool. A wide range of temperature (625K – 1250K) and equivalence ratio (0.5, 1, 2) was considered for this study. All the results for this section are summarized in figures 11 – 15, which presents ignition delay and temporal species profiles for these cases. The ignition is defined when the mixture temperature increases by 400K from initial temperature over one computational time step. According to previous study [43], the other common criteria to define ignition are sharp increases in the OH concentration or rate of temperature increase, gives the same ignition delay time. Figure 11 present the ignition delay time over the range of temperatures and different equivalence ratio. Figure 11a present the ignition delay of one binary blend and two ternary blends with same RON

= 70, but varying S = 0, 4, 5.7. Corresponding results for the blends with RON = 80 is presented in figure 12b.

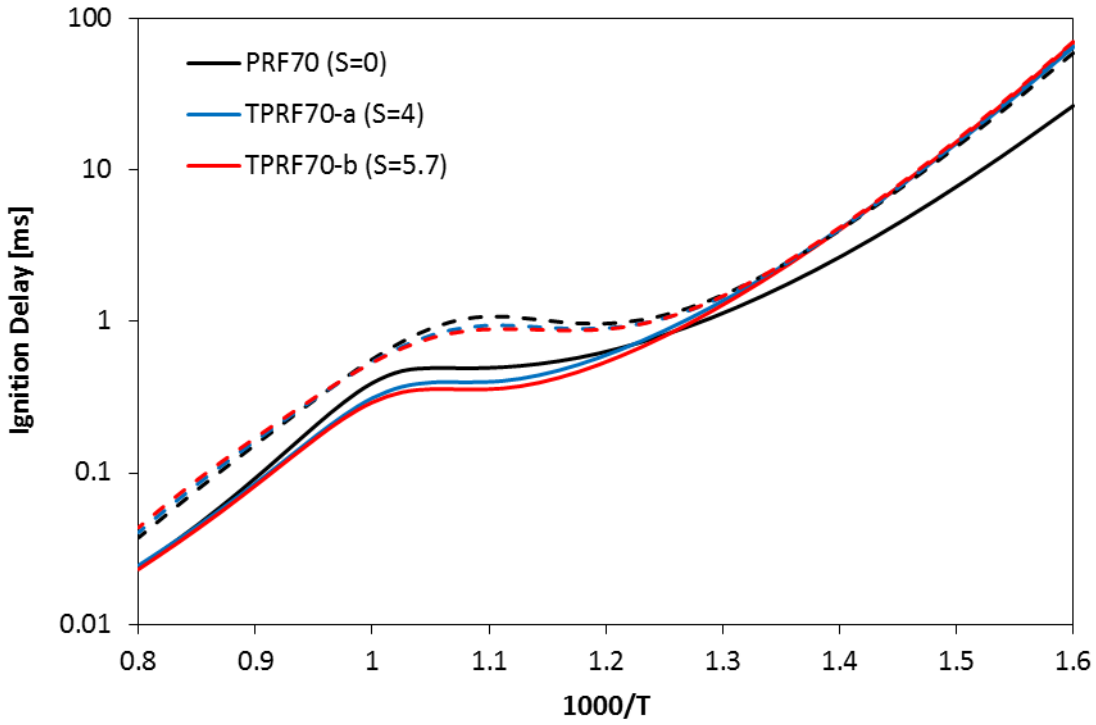

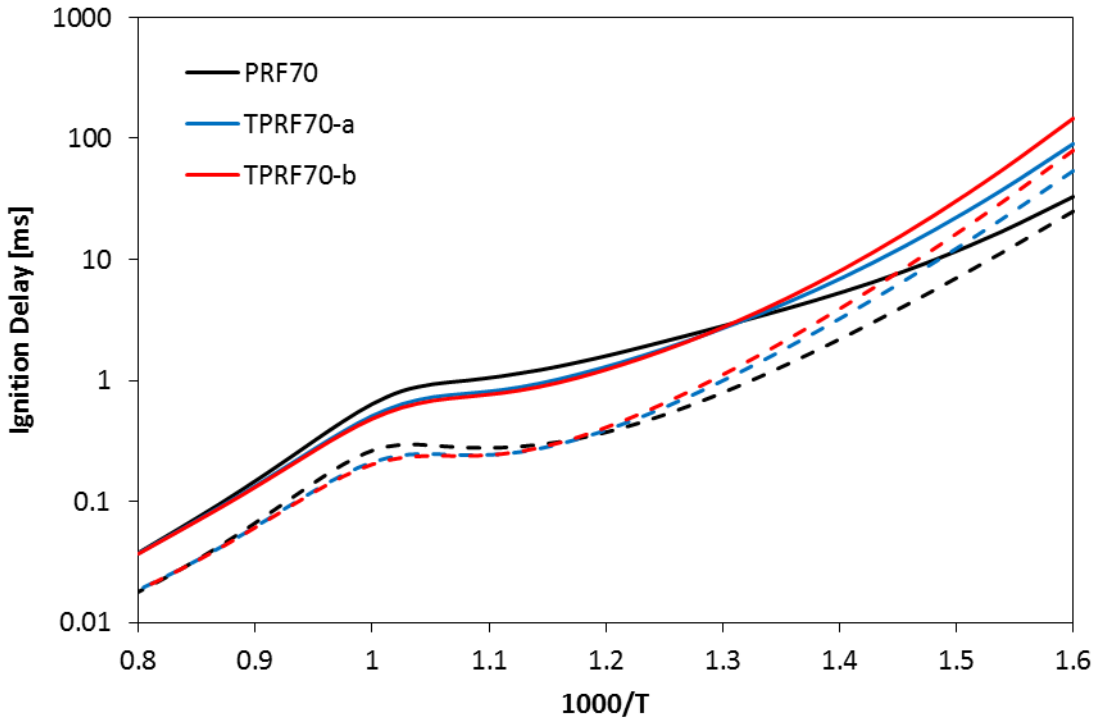

Fig. 11. Ignition delays of blends with RON=70 at P=55 bar (a) ϕ = 1, using the Wang et al. (solid) and LLNL mechanisms (dotted), (b) ϕ=0.5 (solid) and ϕ=2 (dotted).

Results indicate that the fuel sensitivity has a strong influence on the ignition delay for these blends at low (T < 800K) and moderate (800K < T < 1100K) temperatures, but negligible effect at high temperatures (T > 1100K) for both the RON of 70 and 80. At low temperature fuel sensitivity reduces the ignitability of the fuel, i.e. higher ignition delay than the fuel with zero fuel sensitivity. However, at moderate temperatures, the effect is reversed, i.e., an increase in ignitability of the fuel. As shown at moderate temperatures, ternary blends have shorter ignition delay than binary blend fuel. This implies the presence of transition temperature where the effect of fuel sensitivity on ignition is reversed. And as the equivalence is increased, this transition temperature shifts to a higher value. Moreover, all the three blends exhibit NTC region (800K – 1000K), but as the fuel sensitivity is increased, the NTC behavior becomes less pronounced.

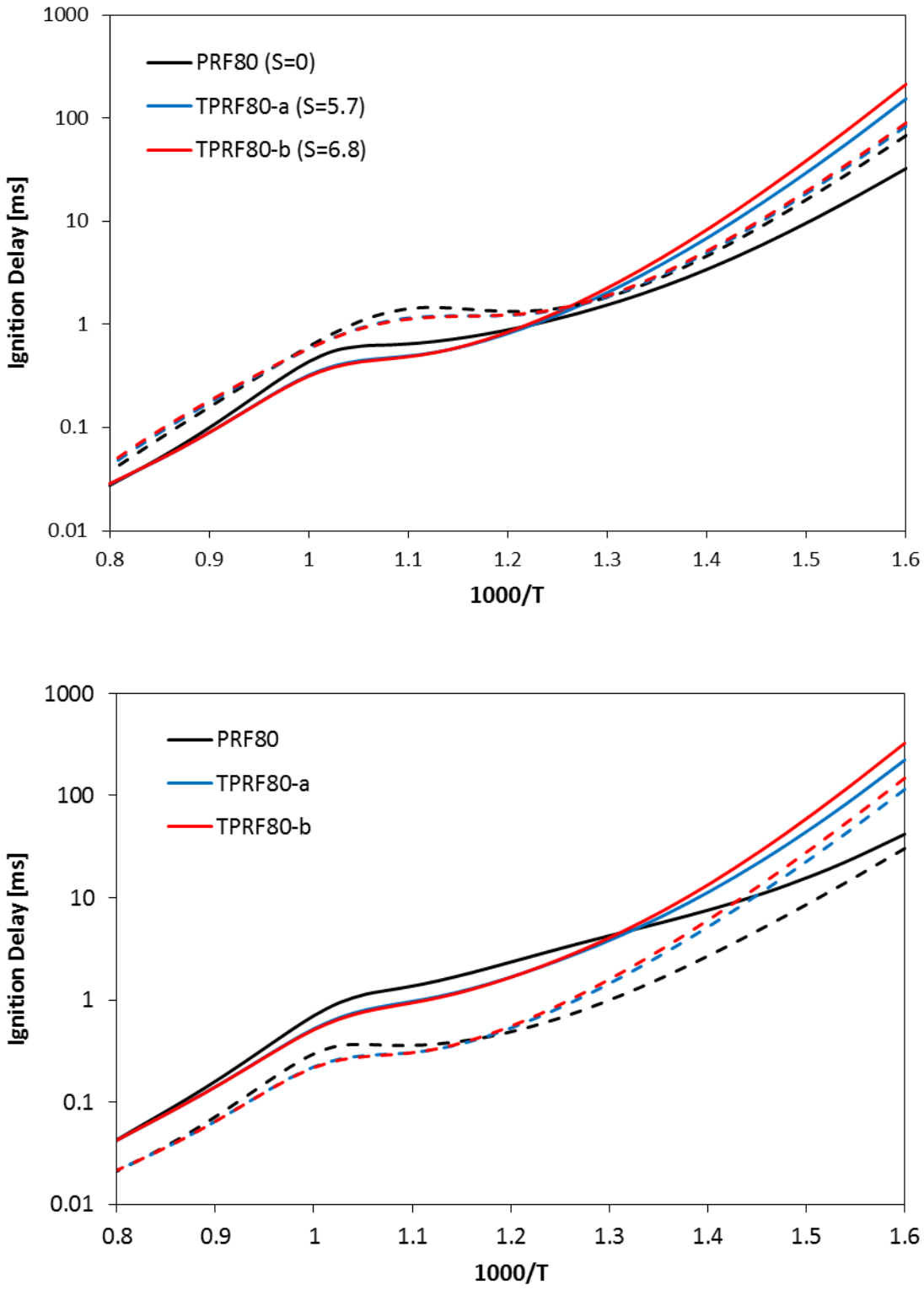

Fig. 12. Ignition delays of blends with RON=80 at P=55 bar (a) ϕ = 1, using the Wang et al. (solid) and LLNL mechanisms (dotted), (b) ϕ=0.5 (solid) and ϕ=2 (dotted).

Further details of the ignition process are provided in Figure 13 – 15 for different initial temperatures (T = 750K, 850K, 1000K). Figure 13 presents the temporal variation of temperature, species concentration and heat release rate (HRR) for the ignition of binary (PRF70) and ternary (TPRF70-a) blends at initial temperature of 750K, pressure P = 55 bar, and equivalence ratio ϕ = 1. The corresponding results for initial temperature T = 850K and 1000K with the same pressure and equivalence ratio are presented in figures 14 and 15, respectively. As shown in figure 13, both binary and ternary blends show the two-stage ignition process. As discussed in previous studies [44, 45], the first stage ignition is defined by the first peak in alkyl hydroperoxyl (QOOH) of heptane and iso-octane mole fractions, or by initial increase in the temperature and HRR.

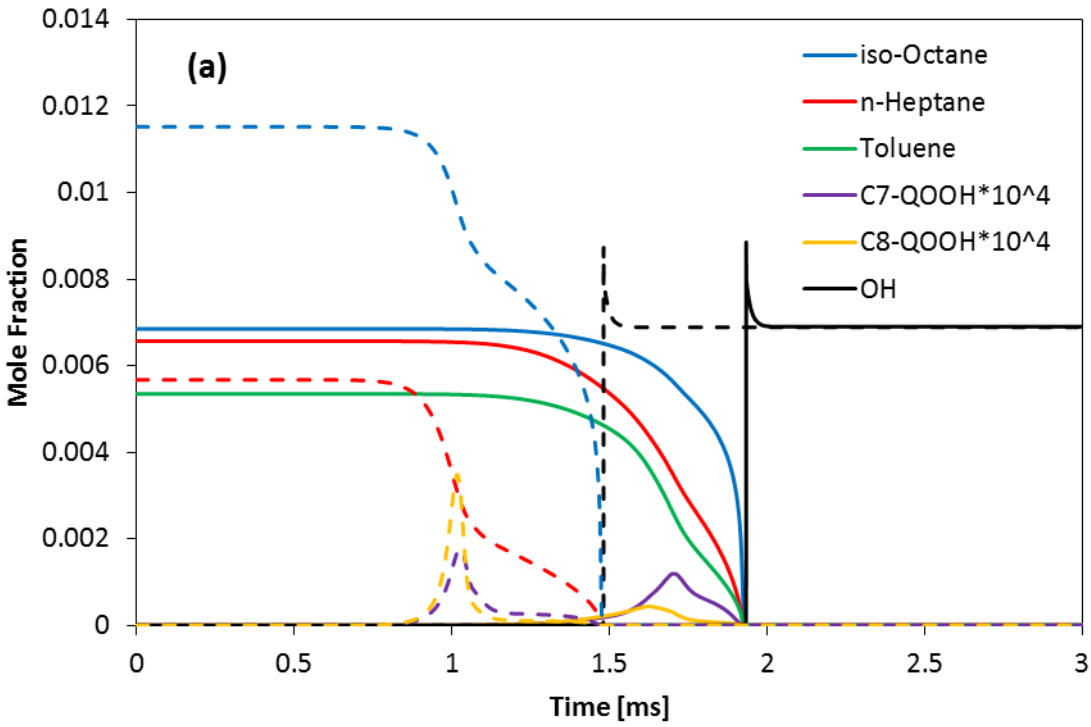

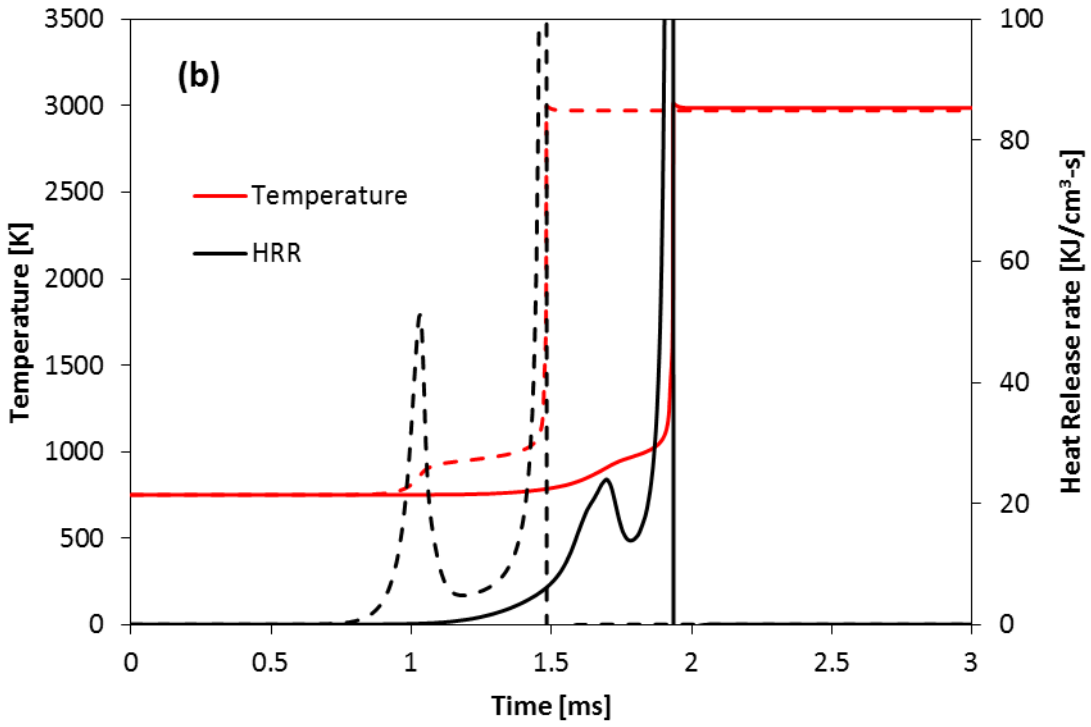

Fig. 13: Temporal species profile (a), and temperature and HRR (b), during the ignition of homogeneous PRF70 (dotted) and TPRF70a (solid) air mixtures at T=750K, P=55 bar, and ϕ=1.

The second or main stage ignition is defined by the sharp increase in OH concentration, temperature and HRR. Results indicate that both the first-stage ignition delay (t1), and second-stage ignition delay (tign) are strongly affected by the fuel sensitivity. The first-stage ignition delays are t1 = 1ms and 1.7ms for PRF70 (S = 0) and TPRF70-a (S = 4) respectively, while the corresponding main-stage ignition delays are tign = 1.45ms and 1.9ms. This shows that the time gap between the first and main ignition events is much smaller for ternary blend compared to the binary blend. Also, the species profile in figure 13 shows that in both binary and ternary blends, the first-ignition process is initiated by the pyrolysis/oxidation of n-heptane, followed by the iso-octane, and finally toluene participates in the ignition process in case of ternary blends. But, this process is delayed due to toluene in ternary blends.

Figure 14 presents the temporal profiles of species, temperature, and HRR during ignition for both binary and ternary blends at initial temperature T = 850K. This temperature pertains to the NTC region. The comparison of this case with the T = 750K case shows that the temperature dependency of ignition delay is strongly affected by fuel sensitivity (S). The first-stage ignition delay times are t1 = 0.19ms and 0.28ms for PRF70 and TPRF70-a respectively, while corresponding main-stage ignition delay times are tign = 0.58ms and 0.51ms. For the case with T=850K, the first stage ignition is longer for ternary blend than that for binary blend, but shorter main-stage ignition delay. This indicates that the blend with high fuel sensitivity exhibits increased ignitability in the NTC region as shown in previous results as well. Similarly figure 15 presents the details of the transient ignition process for both the blends at initial temperature of T = 1000K. At this temperature, the two-stage ignition becomes less pronounced with first stage ignition being relatively weaker and occurring very close to main stage ignition.

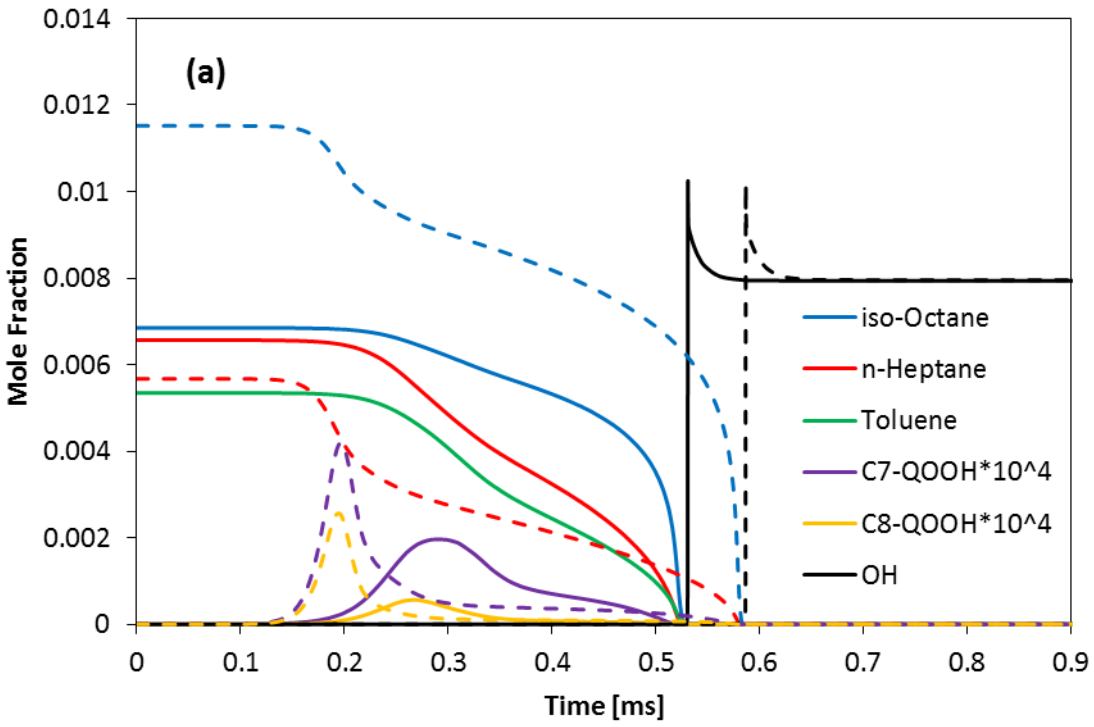

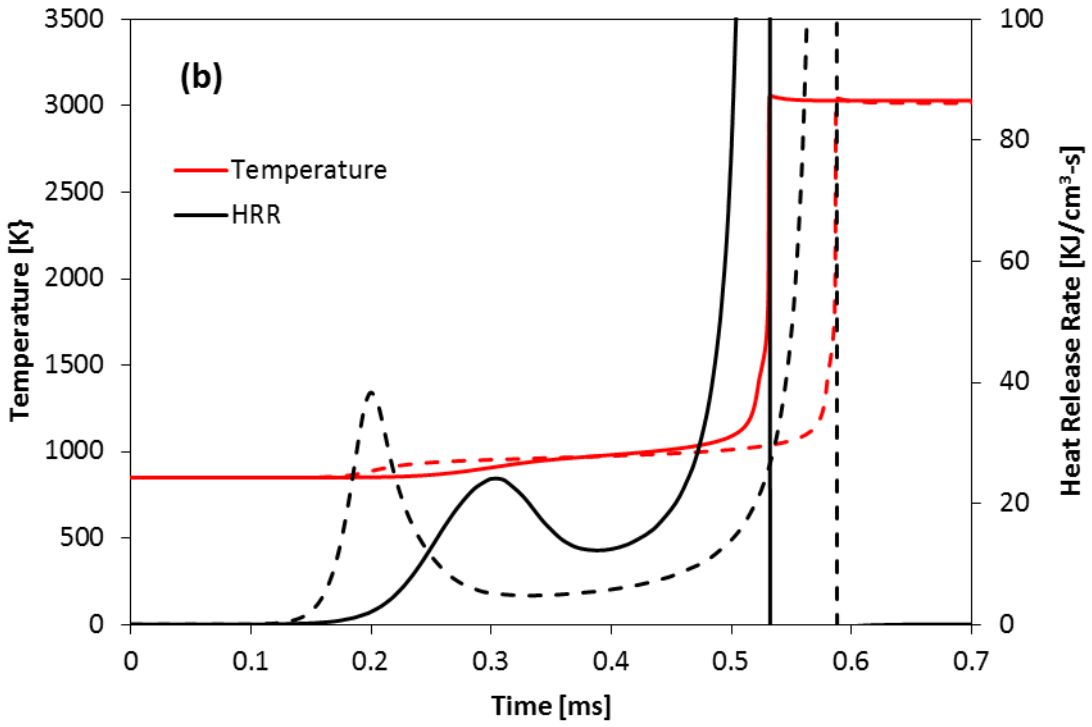

Fig. 14: Temporal species profile (a), and temperature and HRR (b), during the ignition of homogeneous PRF70 (dotted) and TPRF70a (solid) air mixtures at T=850K, P=55 bar, and ϕ=1.

The ignition delays for PRF70 at T = 1000K are t1 = 0.3ms and tign = 0.39ms, and those for TPRF70-a are t1 = 0.25ms and tign = 0.31ms. This shows that the effect of fuel sensitivity is to increase the ignitability. This effect is similar to that at T = 850K. The important observation for the ignition in homogeneous mixture is that the temperature dependence of both the first and main stage ignition process is strongly affected by fuel sensitivity. Thus, at T = 750K, the first and main stage ignition delays for ternary blend (S = 4) are significantly higher than those for binary blend (S = 0). But at T = 850K, the first stage ignition delay of ternary blend is higher, while the main stage ignition delay is lower than that of a binary blend. The ternary blend shows enhanced ignitability in the NTC region. At T = 1000K both first and main stage ignition delay are lower for ternary blend than those for binary blend.

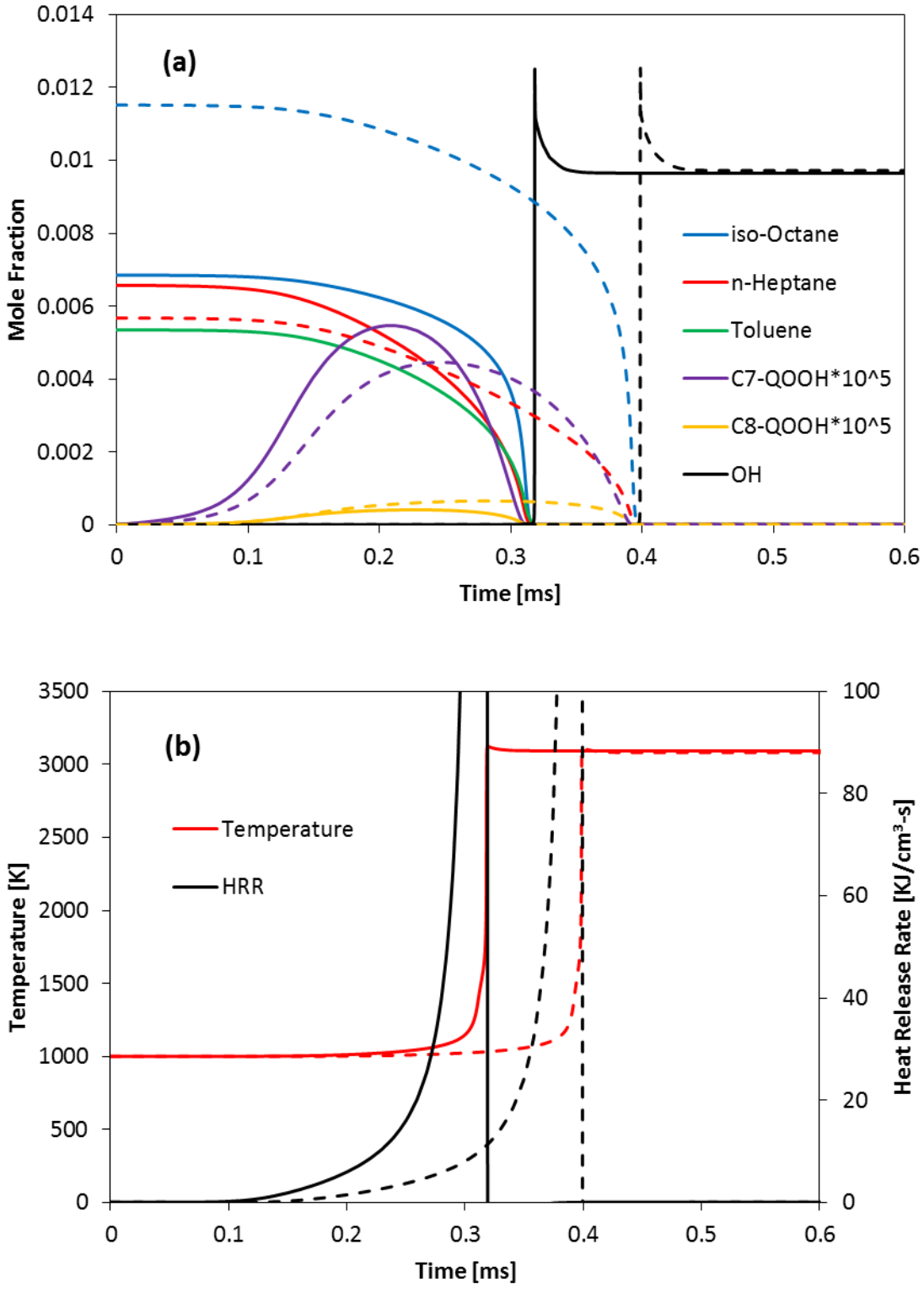

Fig. 15: Temporal species profile (a), and temperature and HRR (b), during the ignition of homogeneous PRF70 (dotted) and TPRF70a (solid) air mixtures at T=1000K, P=55 bar, and ϕ=1.

To identify the important reactions affecting the ignitability of binary and ternary blends, an ignition delay sensitivity analysis was performed. CHEMKIN-Pro was used to identify the important reactions associated with the enhanced ignitability. Figure 16 presents the results of sensitivity analysis for the PRF70 and TPRF70-a at T = 750K and T = 1000K. In figure 16 the reactions with negative sensitivity coefficient promote ignition and vice versa. Reaction R4 involves hydrogen abstraction in which n-heptane is consumed and alkyl radical is formed, promoting ignition.

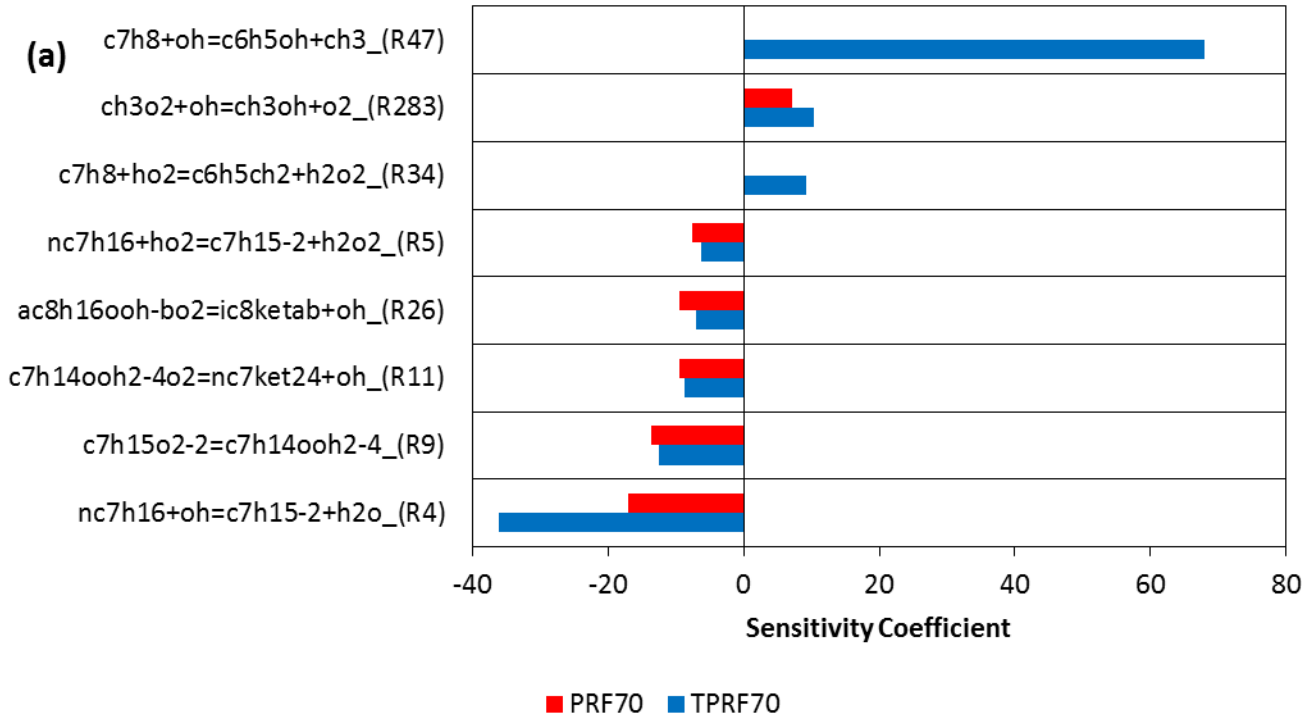

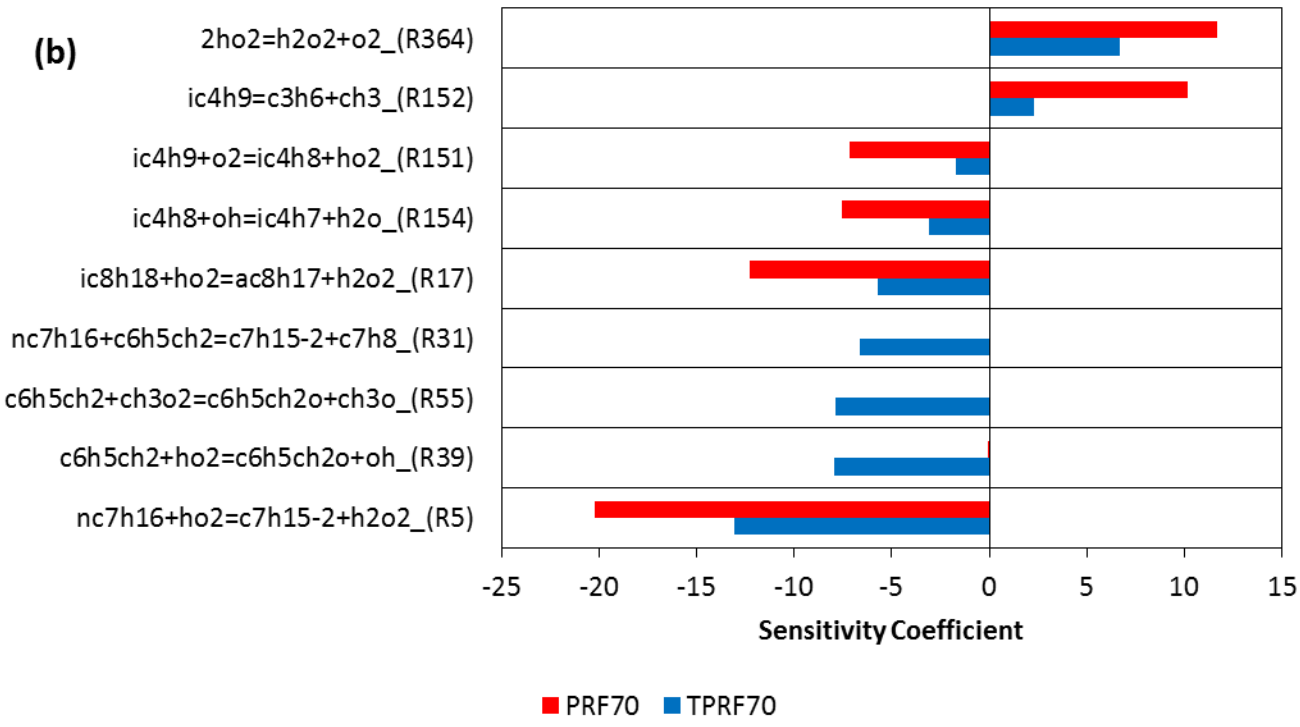

Fig. 16. Sensitivity coefficients computed for PRF70 and TPRF70-a blends at P=55 bar, ϕ=1, and T=750K (a) and T=1000K (b).

As discussed in previous results, ternary blends at low temperatures (T < 800K) have longer ignition delays than binary blends, and this can be examined by the ignition delay sensitivity analysis at T = 750K. As shown in figure 16a, this is primarily due to reaction R47, which has very high positive sensitivity coefficient. Since in this reaction, toluene reacts with OH and produces less reactive species, working as a chain termination reaction, slowing down the ignition process. Similarly, the enhanced ignitability of TPRF70-a is explained by the sensitivity analysis at T = 1000K presented in figure 16b. Three reactions R31, R39 and R55 primarily contribute toward the enhanced ignitability of ternary blends. In reaction R31, n-heptane reacts with toluene alkyl radical to form n-heptyl radical, which is effectively a chain branching reaction, which subsequently leads to the formation of ketohydroperoxide. Similarly, reactions R39 and R55 lead to the formation of C6H5CH2O, which produces OH radicals, and thus promotes ignition.

4.2 **Ignition of Binary and Ternary Fuel Sprays**

(Previously published as Siddharth Kishor Jain and Suresh K. Aggarwal, Compositional effects on the ignition and combustion of low octane fuels under diesel conditions, *Fuel*, 2018, *220*, 654-670 DOI: 10.1016/j.fuel.2018.02.015)

In this section, results focus on the effect of research octane number (RON) and fuel sensitivity (S) on the transient ignition and flame development in sprays. 3-D simulations were performed for two binary blends (PRF70 and PRF80) and two ternary blends (TPRF70-a and TPRF80-a) in Sandia Constant volume reactor at different initial chamber temperatures. Figure 17 presents the ignition behavior of these blends at initial temperatures 900K and 1000K, while table 4 presents the summary of ignition delays of various homogeneous mixture and spray cases. The temporal variation of the volumetric heat release rate (HHR) and fuel species vapor mass for the ignition of PRF70 and TPRF70-a blends at T = 900K and T = 1000K are presented in figure 17a and b, while those for PRF80 and TPRF80-a at T = 1000K are shown in figure 17c. The fuel is initially injected into the reactor at t = 0s.

Table 4. Ignition delay times for homogeneous mixture and spray for different blends and different initial temperatures.

Homogeneous Mixture			
Fuel	Initial Temp (K)	1st Stage Ignition Delay (ms)	Main Ignition Delay (ms)
PRF70	750	1	1.45
TPRF70-a	750	1.7	1.9
PRF70	850	0.19	0.58
TPRF70-a	850	0.28	0.51
PRF70	1000	0.3	0.39
TPRF70-a	1000	0.25	0.31
Spray			
Fuel	Initial Temp (K)	1st Stage Ignition Delay (ms)	Main Ignition Delay (ms)
PRF70	900	0.39	2.7
TPRF70-a	900	0.59	1.2
PRF70	1000	0.27	0.92
TPRF70-a	1000	0.37	0.67
PRF70	1100	0.21	0.49
TPRF70-a	1100	0.24	0.43
PRF80	1000	0.36	1.37
TPRF80-a	1000	0.47	0.83

Following atomization, the vaporization process is initiated. Thus, as shown in figure 17a, the fuel species vapor mass increases with time. As fuel vapor mixes with air at high temperature and pressure in constant volume, the chemical reactions are initiated leading to ignition. For both binary and ternary blends, HRR profiles is used to define two-stage ignition. The first initial increases in HRR indicates the first stage ignition, with the first stage ignition delays being 0.39ms and 0.59ms for the PRF70 and TPRF70-a respectively. The first stage ignition can also be identified by the change in slope in n-heptane and toluene vapor mass profiles. The first stage ignition of PRF70 is mainly initiated by the pyrolysis/oxidation of n-heptane, while that of TPRF70-a involves both n-heptane and toluene. The second-stage or main ignition is indicated by the second sharp increase in HRR or a sudden drop in fuel vapor mass. The main stage ignition delays for PRF70 and TPRF70-a blends are 2.7ms and 1.2 respectively. And for the corresponding results for T = 1000K shown in figure 17b, the first stage ignition delays are 0.27ms and 0.37ms for PRF70 (S = 0) and TPRF70-a (S = 4) respectively, while main stage ignition delays are 0.92ms and 0.67ms, respectively. These two results clearly demonstrate the temperature dependency of spray ignition on fuel sensitivity. As temperature is increased from 900K to 1000K the first stage ignition as well as main stage ignition delays decreases for both the blends. But the effect of temperature on main stage ignition is more pronounced for PRF70. The peak HRR for PRF70 is higher than the TPRF70, which is due to the much longer ignition delay resulting in more fuel evaporation for PRF70 blend.

The effect of RON on main ignition is presented in figure 17c, which plots results for PRF80 (S = 0) and TPRF80-a (S = 5.7) at T = 1000K, and these should be compared with the results of RON = 70 blends in figure 17b. The main ignition delays are 1.37ms and 0.83ms for PRF80 and

TPRF80-a, respectively, while those for PRF70 and TPRF70-a are 0.92ms and 0.67ms respectively. This shows that the ignition delay is increased with the increase in RON.

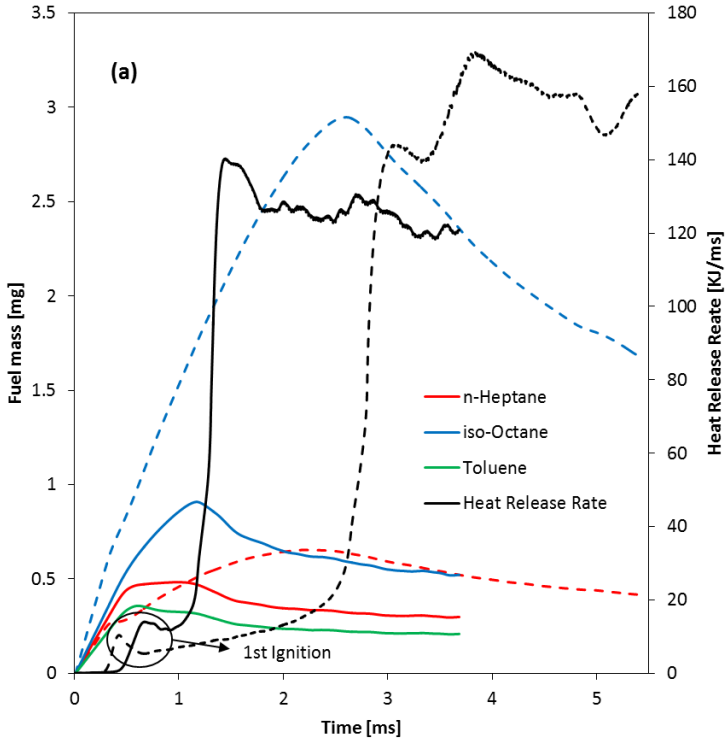

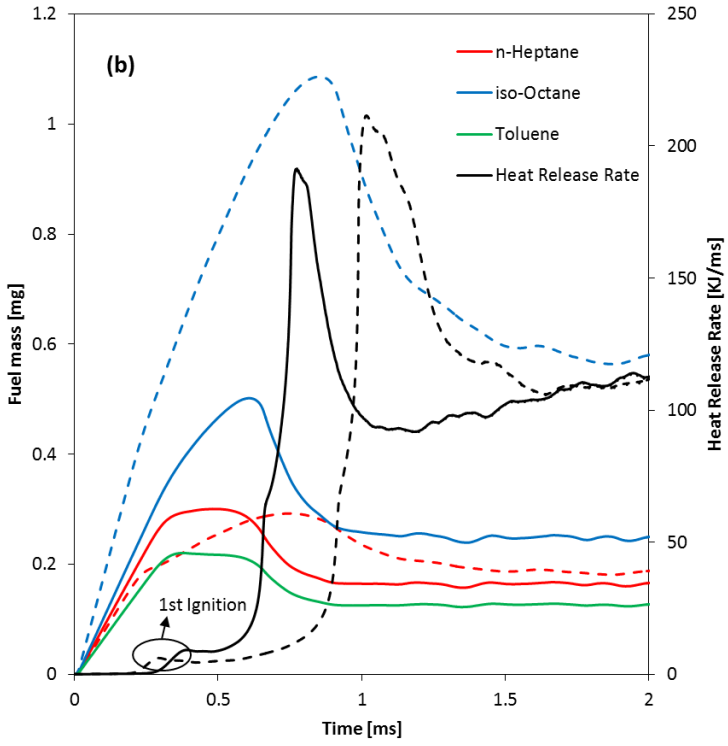

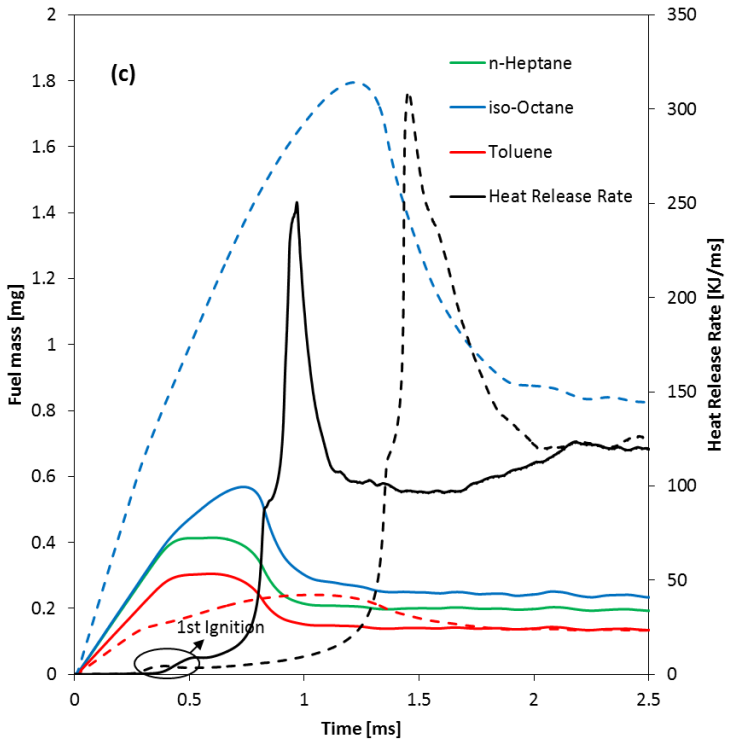

Fig. 17. Temporal profiles of integrated fuel vapor mass and heat release rate for the ignition of binary and ternary blends at different temperatures. Fig. (a) PRF70 (dotted) and TPRF70-a (solid) blends at 900K, Fig. (b) PRF70 (dotted) and TPRF70-a (solid) blends at 1000K, and Fig. (c) PRF80 (dotted) and TPRF80-a (solid) blends at 1000K.

When the spray ignition results are compared with those for homogeneous mixture regarding the effect of RON and S, it is observed that the ignition delay time is noticeably higher in sprays due to the effects of vaporization and temporally and spatially developing two-phase flow field. Vaporization absorbs heat initially, decreasing the mixture temperature for pyrolysis/ oxidation reactions. This affects both the first and main stage ignition processes in spray ignition. Due to this, the effective spray ignition temperature is reduced, and effective equivalence ratio may be higher or lower depending upon the spray behavior. This implies that the effect of S on ignition may be modified in sprays compared to homogeneous mixtures. This is shown by the ignition delay in Table 4; for homogeneous mixture the effect of S is to increase both the first

stage and main stage ignition delays at T = 750K with the increase of S, but at T = 850K, the first stage is increased, while the main stage ignition delay is decreased. At higher temperatures in homogeneous mixtures, both the first stage and main stage ignition delays are decreased due to the effect of sensitivity. This shows the effect of fuel sensitivity on the temperature dependency of the first stage and main ignition delays. This is also observed in spray ignition. The effect of S at 900K in spray ignition is to increase the first stage ignition while decreasing the main stage ignition delay similar to that for homogeneous mixture at 850K. A similar behavior is observed for spray ignition of RON = 70 and 80 at 1000K. But there are differences between homogeneous mixture and spray results. The effect of S in homogeneous mixture at low temperatures is to increase both first and main stage ignition, at moderate temperature, it increases first stage ignition but decrease main stage ignition, while at high temperature, it decreases both the first and main stage ignition delay times. Thus, a transition temperature is observed for ignition in homogeneous mixtures. But for the range of temperatures used to study spray ignition, the effect of S is to increase the first stage ignition delay and decrease the main stage ignition delay. Thus, the transition temperature is not observed for spray ignition. This may be due to the temporally and spatially developing two-phase flow field, which modifies the effective temperature and equivalence ratio in the ignition kernel for sprays. It should also be noted that temperatures below 900K could not be investigated for sprays due to prohibitively long ignition delays for 3D simulations.

4.3 **Transient Ignition and Flame Development in Binary and Ternary Fuel Sprays**

(Previously published as Siddharth Kishor Jain and Suresh K. Aggarwal, Compositional effects on the ignition and combustion of low octane fuels under diesel conditions, *Fuel*, 2018, *220*, 654-670 DOI: 10.1016/j.fuel.2018.02.015)

In this chapter, we present the temporal and spatial details of spray ignition kernel and subsequent flame development in figures 18 – 21. Figure 18 presents the first stage ignition kernel in terms in C7-QOOH scatter plot in ϕ-T space for binary and ternary blends at initial temperature T = 900K and 1000K.

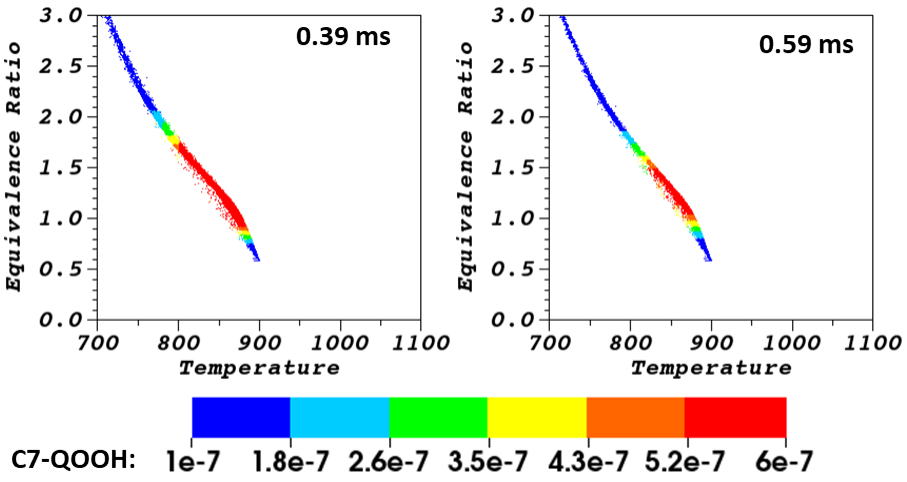

a: PRF70 (left) and TPRF70-a (right) at T=900K

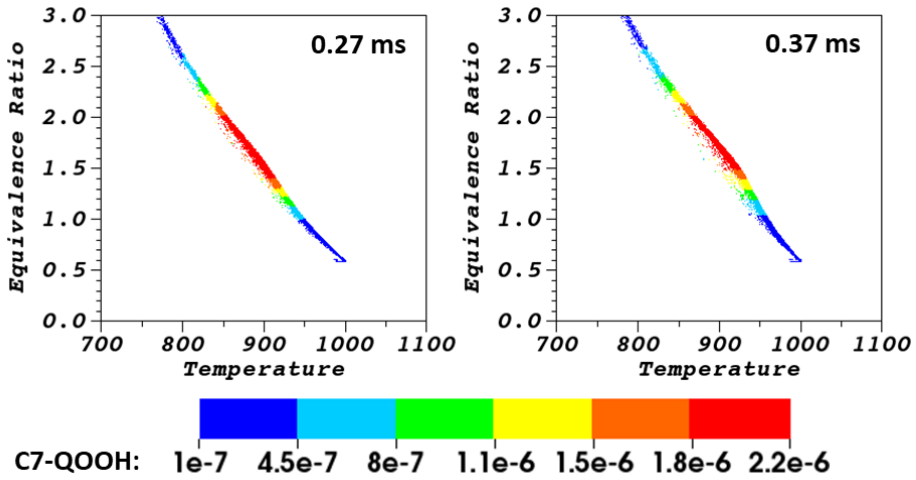

b: PRF70 (left) and TPRF70-a (right) at T=1000K

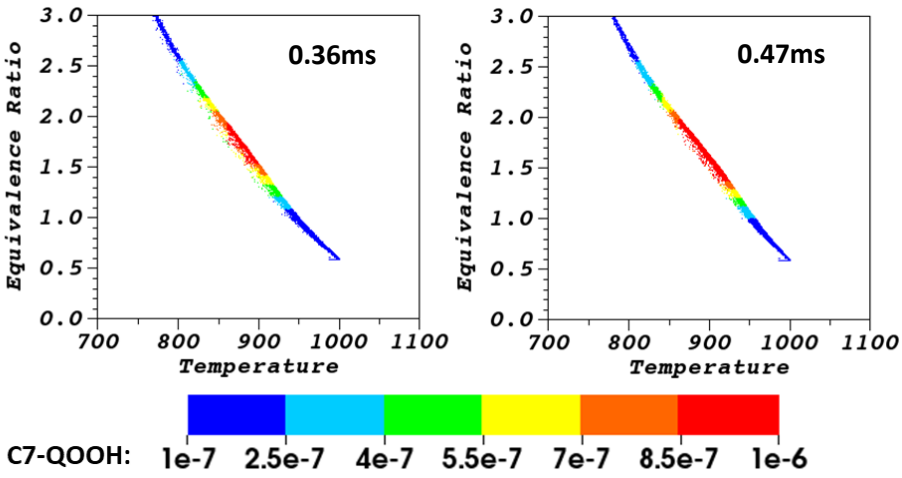

c: PRF80 (left) and TPRF80-a (right) at T=1000K

Fig. 18. First stage ignition depicted through scatter plots of C7-QOOH mass fraction in ϕ-T space for various binary and ternary blends; (a) PRF70 (left) and TPRF70-a (right) blends at 900K, (b) PRF70 (left) and TPRF70-a (right) blends at 1000K, (c) PRF80 (left) and TPRF80-a (right) blends at=1000K.

Fu and Aggarwal [39, 44] presented similar scatter plots in their study to describe the spray ignition and combustion characteristic. In Fu and Aggarwal [39, 44] study and this study equivalence ratio is defined as

$$\phi = \frac{2\sum_{xs} N_i X_{C,i} + \frac{1}{2}\sum_i N_i X_{H,i}}{\sum_i N_i X_{O,i}} \quad \ldots(11)$$

Where the summation is over all species (xs) excluding CO2 and H2O, Ni is the number of moles of species i and XC,i, XH,i, and XO,i the number of carbon, hydrogen and oxygen atoms in $i\,th$ species.

Figure 18a and 18b present the scatter plots for PRF70 and TPRF-a blends at 0.39ms and 0.59ms respectively for T = 900K and 1000K, respectively. Similar plots for PRF80-a and TPRF80-a blends are presented in figure 18c at T = 1000K. All the time values in figure 18 refer to first stage ignition delay of the respective blends. In all the cases presented in figure 18, except for

the differences in ignition delay times, the first stage ignition process is qualitatively similar. The first stage ignition occurs over a wide range of equivalence ratios ($\phi \approx 1 - 2.1$) but a narrow range of temperatures (825K – 900K). This wide range of equivalence ratio is due to the difference in ignition time causing different level of fuel-air mixing. Also, it is interesting to observe that the mixture temperature is lower than the initial temperature, which is due to the process of vaporization.

Similarly, main-stage ignition and subsequent flame structure for these blends are presented in terms of HRR in figure 19. Figure 19a presents the main-stage ignition and flame structure in ϕ-T space for PRF70 and TPRF70-a at T = 900K, and that of T = 1000K is plotted in figure 19b. Similarly, the main-stage ignition and flame structure for PRF80 and TPRF80-a at T = 1000K are presented in figure 19c. In figure 19a the main-stage ignition kernel is characterized by a small region with HRR near T = 1400K. Results indicate that the main ignition kernel is formed at stoichiometric mixture ($\phi \approx 1$) for PRF70, while that for TRPF70-a is formed comparatively at richer mixture ($\phi \approx 1.25$). This difference is associated with the difference in ignition delay times, with shorter ignition delays and thus less fuel-air mixing for ternary blends. A similar trend is observed in figure 19b, which presents the main-stage ignition kernel and flame structure for PRF70-a and TPRF70-a at T = 1000K. The main-stage ignition delays for PRF70 and TPRF70-a are 0.92ms and 0.67ms respectively. As the initial temperature is increased from 900k to 1000K, the ignition kernels for both blends are associated with richer mixtures. The HRR scatter plots for of PRF80 and TPRF80-a at 1.37ms and 0.83ms, respectively, in figure 19c, indicate a similar effect of fuel sensitivity on the ignition kernel. The blue region in the scatter plots implies negative HRR, indicating the pre-ignition endothermic reactions.

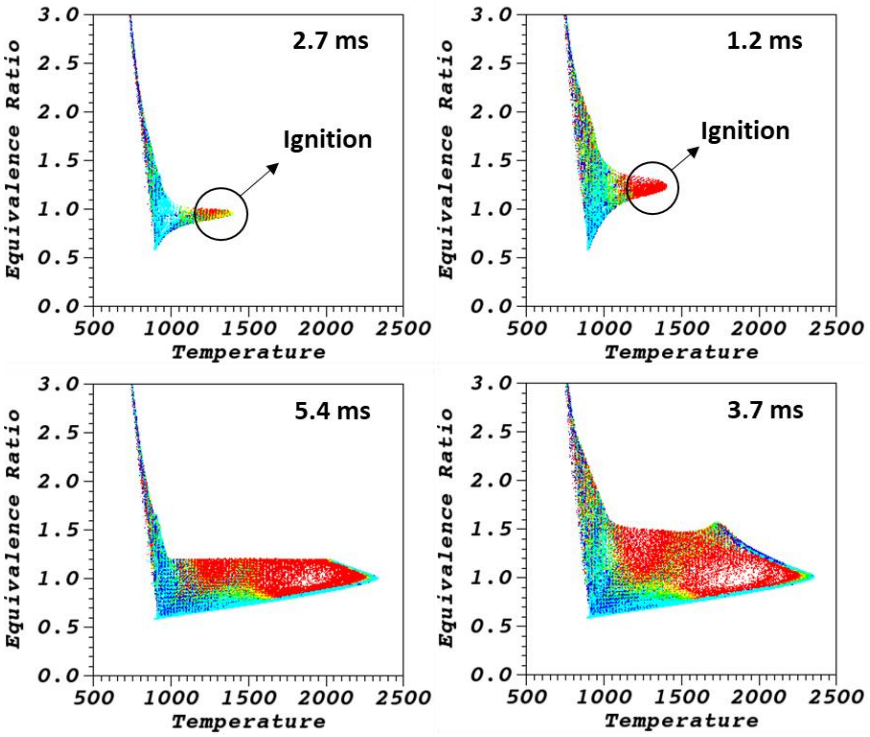

a: PRF70 (left) and TPRF70-a (right) at T=900K

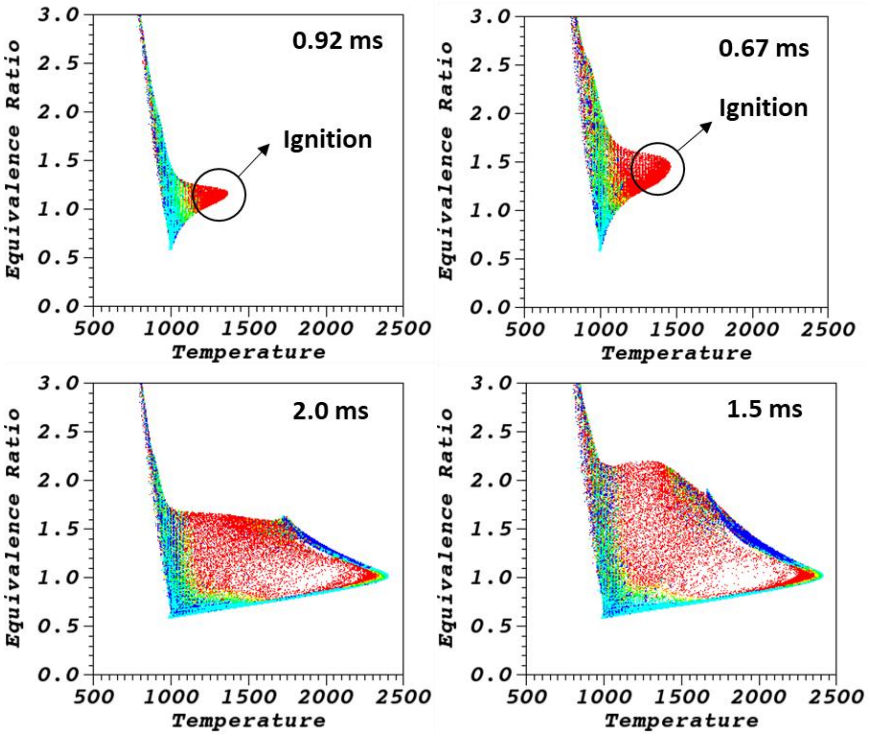

b: PRF70 (left) and TPRF70-a (right) at T=1000K

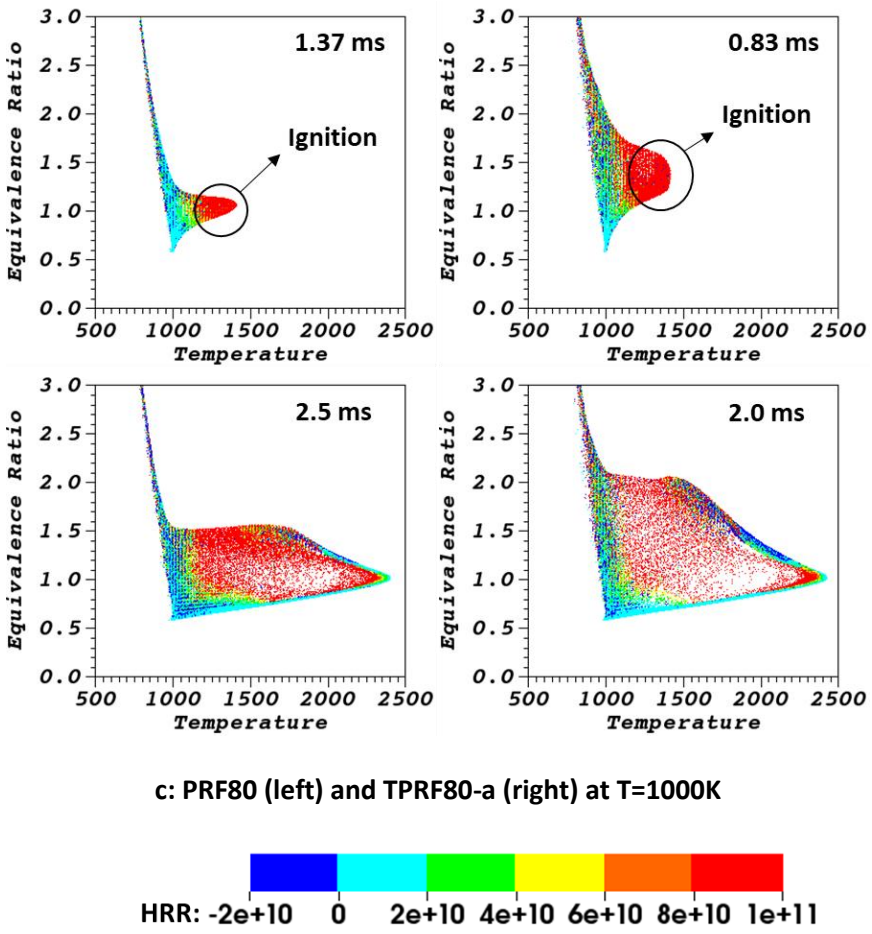

c: PRF80 (left) and TPRF80-a (right) at T=1000K

Fig. 19. Scatter plots of HRR (J/m3/s) in ϕ-T space at different times after SOI, showing the ignition kernel and flame structure in PRF (left) and TPRF (right) sprays at for different RON and initial temperatures; (a) RON=70 and T=900K, (b) RON=70 and T=1000K, (c) RON=80 and T=1000K.

The HRR scatter plots at later times in figure 19 indicate that the flame structure for these blends is characterized by partially premixed combustion involving three reaction zones, namely lean premixed zone (LPZ), non-premixed zone (NPZ) and rich premixed zone (RPZ). For PRF70 at 900K, Fig. 19a indicates a LPZ ($\phi \approx 0.8$, 1500K<T<2000K) and NPZ ($\phi \approx 1$, 1900K<T<2300K), with a relatively weak RPZ. This is due to long ignition delay time, providing more time for fuel-air mixing. Similarly, the plot for ternary blend at 3.7ms indicates the existence of LPZ ($\phi \approx 0.8$, 1500K<T<2000K), NPZ ($\phi \approx 1$, 1900K<T<2300K), and RPZ (1.2<ϕ<1.5, 1300K<T<1700K). As the

initial temperature is increased to 1000K, the three reaction zones are noticeably modified. Scatter plot for PRF70 at 1000K at 2ms in figure 19b indicates that at higher temperatures with comparatively shorter ignition delay, the flame involves a significant contribution from RPZ in addition to LPZ and NPZ. Similarly, the flame for TPRF70-a at 1000K involves richer mixture in RPZ ($1.4<\phi<2.0$) compared to that of PRF70. The scatter plots for PRF80 and TPRF80-a at T = 1000K are qualitatively similar to PRF70 and TPRF70-a respectively. In summary, the effect of fuel sensitivity is to increase the ignition delay time, which also modifies the ignition kernel and flame structure. For instance, PRF's ignition kernel occurs near stoichiometric mixture, while TPRF's ignition kernel occurs in a richer mixture. And also, the flame structure for ternary blend involves higher contribution of RPZ.

Further details of ignition kernel and flame structure in the physical space are presented using temperature color contours and equivalence ratio (ϕ) line contours in figure 20 and 21. Figure 20 presents the contours these showing the ignition and temporal flame progression for the PRF70 spray at initial temperature T = 900K. The contours are plotted at the center cut plane in a cropped region (0.05x0.1 m2) of the 3-D computational domain (0.108x0.06x0.06 m3) simulating the Sandia reactor. The contours at 2.7ms refer to the ignition kernel corresponding to the temperature 1300K and near equivalence ratio of 1, while contours at later time showt the temporal development of flame with multiple reaction zones. Figure 21 presents the equivalence ratio and temperature contours during ignition and well-developed flame for various blends and at different initial temperatures. Figures 21a and b present results for PRF70 and TPRF70-a at 900K and 1000K respectively, while results for PRF80 and TPRF80-a at 1000K are presented in figure 21c.

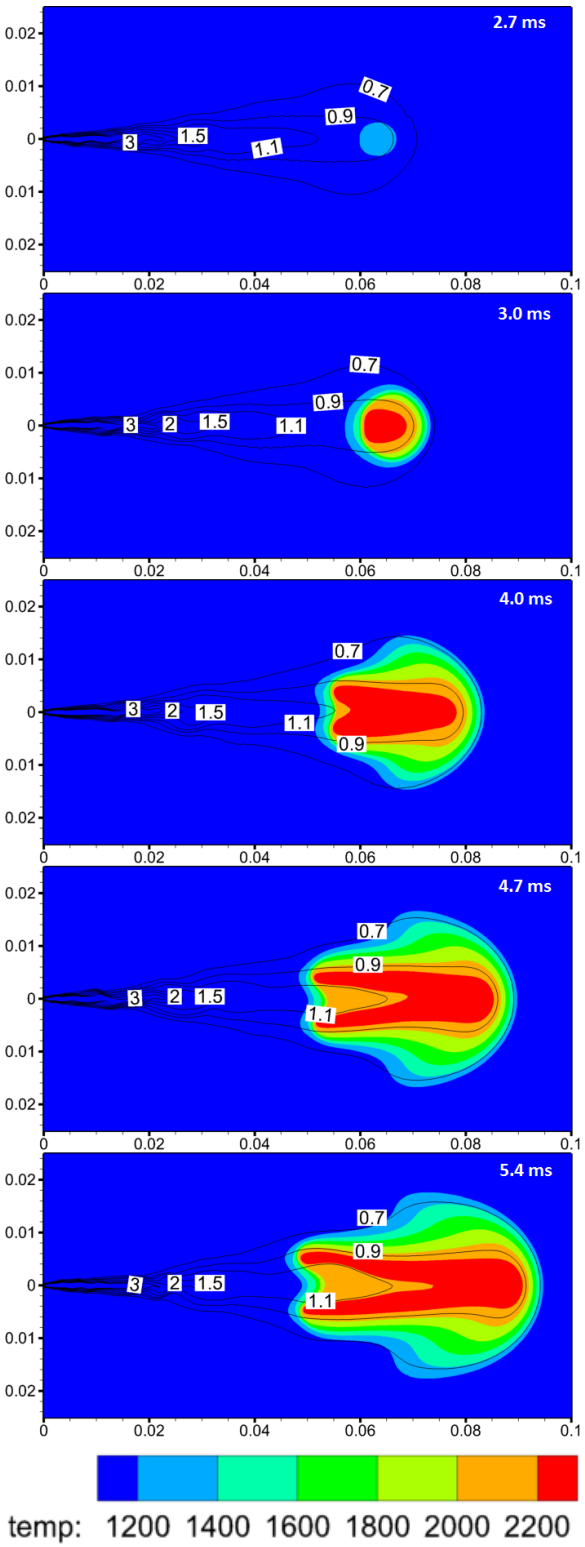

Fig. 20. Equivalence ratio (ϕ) and temperature contours at the center cut plane at different times after the start of injection (SOI), showing the temporal evolution of PRF70 spray flame at T=900K. Color contours represent temperatures 1100-2400K. Black contour lines with labels indicate ϕ values. Dimensions are in m. For this case, main ignition occurs at 2.7ms.

Figure 21a at 2.7ms and 1.2ms shows the main stage ignition of PRF70 and TPRF70-a. As noted earlier with reference to HRR scatter plots, the fuel sensitivity (S) increases the ignitability, and consequently, the ignition occurs earlier and in rich mixture ($\phi \approx 1.25$) for TPRF70-a. In contrast, for binary blends, the longer ignition delay facilitates more fuel-air mixing, and thus ignition occurs near stoichiometric mixture. Subsequently, the ignition kernel develops into flame for both blends. The contours at 5.4ms and 3.7ms characterize a nearly developed flame for the binary and ternary blends, respectively. Note that the vertical green line indicates the flame lift-off length. As shown in figure 21a, the flame lift-off length for TPRF70-a is comparatively shorter (0.037m) than that for PRF70 (0.048m). A similar behavior is observed for all the cases at different initial temperatures. This is consistent with the results reported by Sharma and Aggarwal [45] that the lift-off length is mainly controlled by the ignition process, i,e., shorter ignition delay time leads to shorter lift-off length. Results for PRF70 and TPRF70-a at 1000K are presented in figure 21b. Consistent with HRR scatter plots discussed earlier, the ignition for PRF70 occurs at 0.92ms and in near stoichiometric mixture ($\phi \approx 1.1$), while that for TPRF70-a occurs at 0.67ms and a richer mixture ($\phi \approx 1.4$). The contour at 2ms and 1.5ms depict the developed flames for PRF70 and TPRF70-a at 1000K. Results indicate that the flames for both the blends are characterized by three reactions zones, i.e., LPZ, RPZ, and NPZ. Moreover, the lift-off length follows the same trend with PRF70 having longer lift-off length due to longer ignition delay. The contour plots for PRF80 and TPRF80-a at T = 1000K, presented in figure 21c, indicate that blends with RON = 80 follow the same trend as blends with RON = 70, except for the difference in ignition delay times. The main difference is that for blends with RON = 80, the lift-off length is longer due to longer ignition delay.

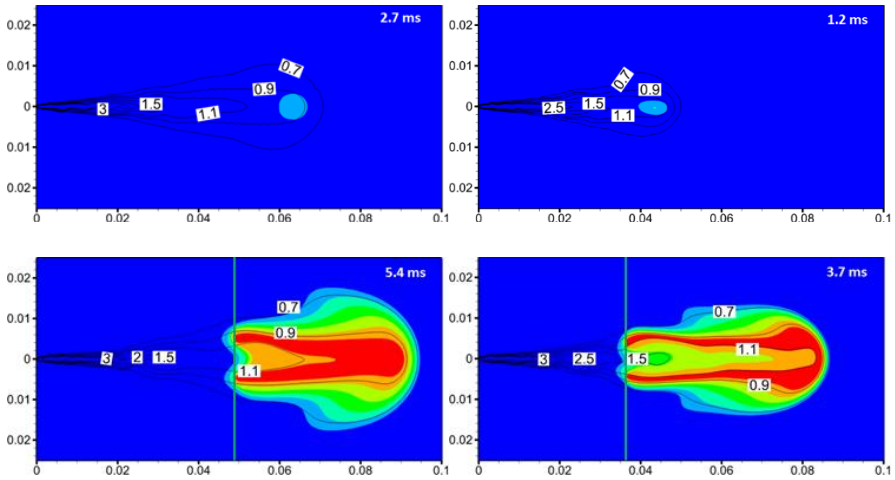

a: PRF70 (left) and TPRF70-a (right) at T=900K

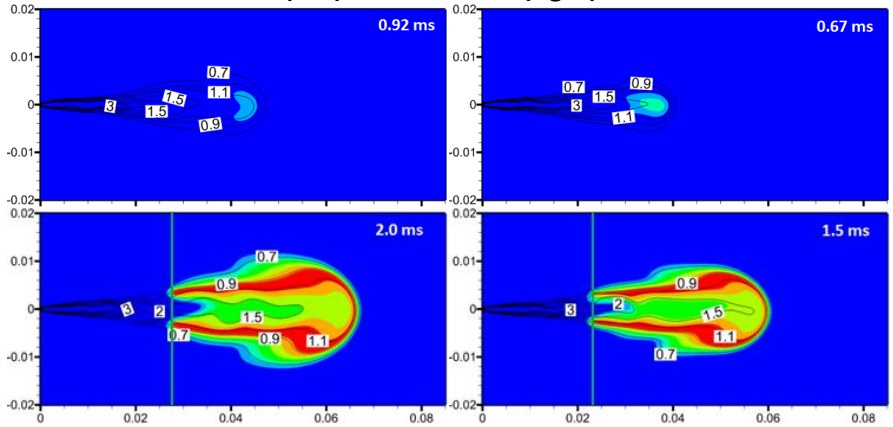

b: PRF70 (left) and TPRF70-a (right) at T=1000K

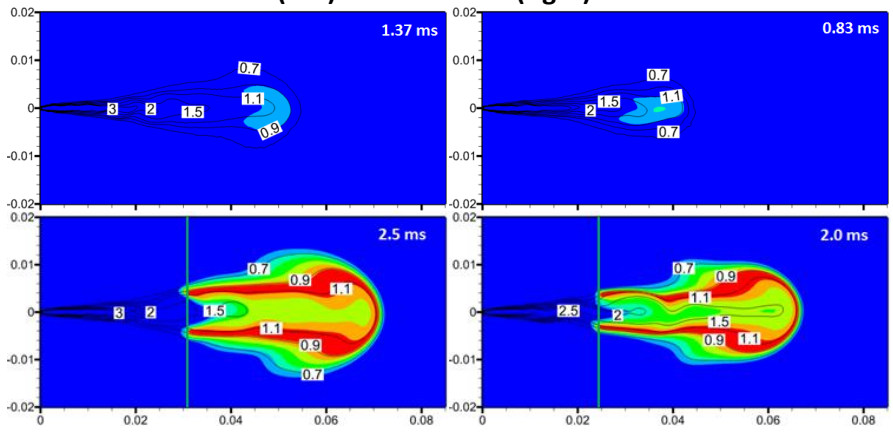

c: PRF80 (left) and TPRF80-a (right) at T=1000K

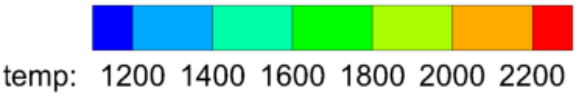

Fig. 21. Equivalence ratio (ϕ) and temperature contours showing the ignition kernel and flame structure in PRF (left) and TPRF (right) sprays for different RON and initial temperatures. (a) RON=70 and T=900K, (b) RON=70 and T=1000K, (c) RON=80 and T=1000K. Color contours represent temperatures 1100-2400K. Black contour lines with labels indicate ϕ values. Dimensions are in m.

Various reaction zones can be further differentiated by using scatter plots of relevant species in ϕ-T space. Following Fu and Aggarwal [39], figure 22 presents scatter plots of NO2, OH, and C2H2 characterizing the lean premixed zone (LPZ), non-premixed zone (NPZ) and rich premixed zone (RPZ), respectively for PRF70a and TPRF70-a at T = 1000K. NO2 is mostly formed in LPZ due to the availability of abundant O2, as indicated in figure 22a. Similarly, figures 22b and 22c present the scatter plot of OH and C2H2 respectively. Both LPZ and NPZ are qualitatively similar for PRF70 and TPRF70-a, except RPZ for PRF70a is weaker than that for TPRF70-a. This is due to longer ignition delay facilitating more fuel-air mixing. LPZ is characterized by ϕ≈0.7-0.8, and T≈1300-1700K, and NPZ by ϕ≈0.9-1.1 and T≈2000-2400K.

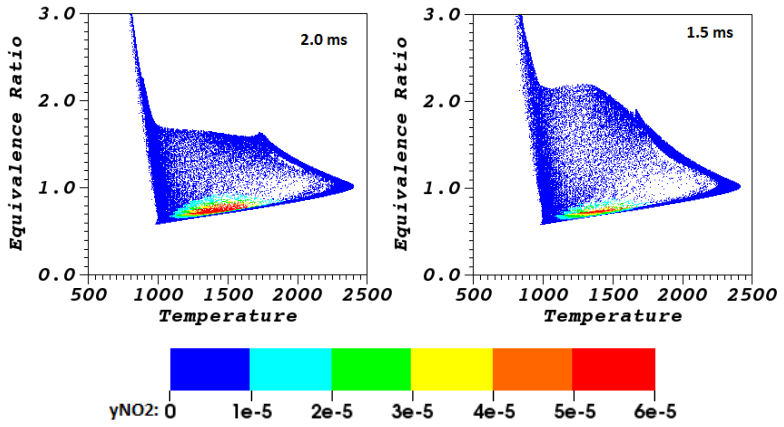

(a): NO2 depicting the lean premixed zone (LPZ) in PRF70 (left) and TPRF70-a (right) flames

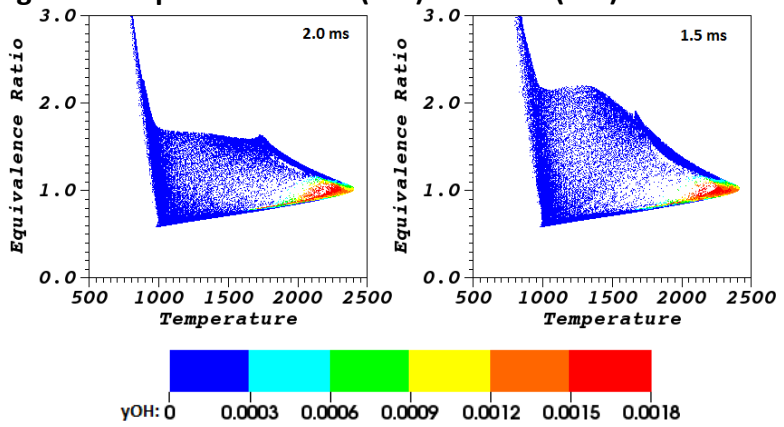

(b): OH depicting the non-premixed zone (NPZ) in PRF70 (left) and TPRF70-a (right) flames

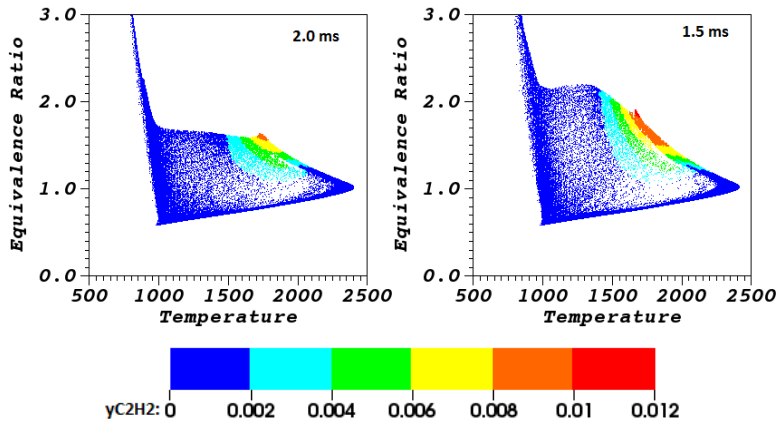

(c): C2H2 depicting the rich premixed zone (RPZ) in PRF70 (left) and TPRF70-a (right) flames

Fig. 22. Scatter plots of species mass fractions in ϕ-T space at different times after SOI, depicting the three reaction zones for different blends; (a) NO2 scatter plots, (b) OH scatter plots, (c) C2H2 scatter plots. Initial temperature=1000K.

4.4 Effect of Fuel Sensitivity (toluene) on PAH formation in Partially Premixed Flames

In this section, results are presented for PRF70, TPRF70-a and TPF70-b partially premixed counterflow flames, to focus on the effects of fuel sensitivity on the flame structure and PAH formation. Figure 23 presents the flame structure and PAH species profile of PRF70 partially premixed counterflow flame. The flame structure is characterized by axial profiles of heat release rate (HRR), flame temperature and velocity in figure 23a, while figure 23b presents the PAH profiles. The flame structure is characterized by two reaction zones, as indicated by the two peaks in HRR profile, one corresponding to the rich premixed zone (RPZ) which is located on the fuel side and the other indicating the non-premixed reaction zone (NPZ) is located close to the stagnation plane. The stagnation plane, RPZ and NPZ are highlighted by solid, dashed and dotted vertical lines in figure 23, respectively.

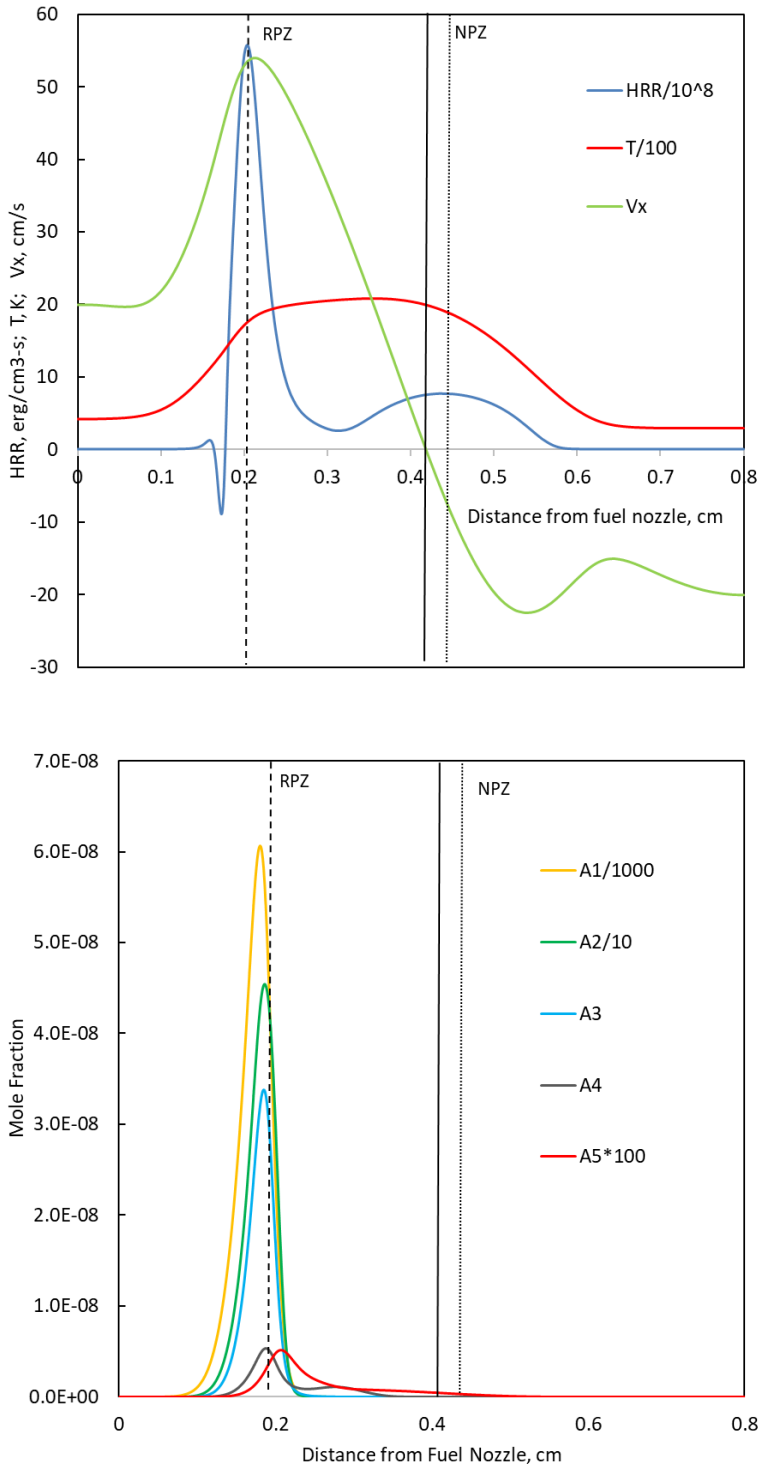

Fig. 23: Flame structure of PRF70 partially premixed flame at ϕ = 2. (a) Temperature, HRR, axial velocity, and (b) PAHs mole fractions. Vertical lines represent the locations of rich premixed zone (RPZ), stagnation plane and non-premixed zone (NPZ).

For partially premixed counterflow flames, fuel typically undergoes pyrolysis and oxidation reactions in the RPZ to form CO, H2 and other hydrocarbon species [21, 24], while CO and H2 are then oxidized to form CO2 and H2O near the NPZ/stagnation plane. PAHs species peak near RPZ (fuel rich side) with A1 peaking first, and then followed by larger PAH compounds which are eventually consumed in the same order between RPZ and stagnation plane, but closer to RPZ. Figure 24 and 25 show the flame structures for TPRF70-a and TPRF70-b ternary blends, respectively. The flame structures appear to be similar to that for the PRF70 blend in terms of the formation of two reaction zones (RPZ, NPZ), location of stagnation plane, distance between reaction zones, etc. The nature of PAH species profiles is quite similar as well. However, it is important to note that the PAHs concentrations vary considerably, with significantly higher values in TPRF70-a and TPRF70-b flames.

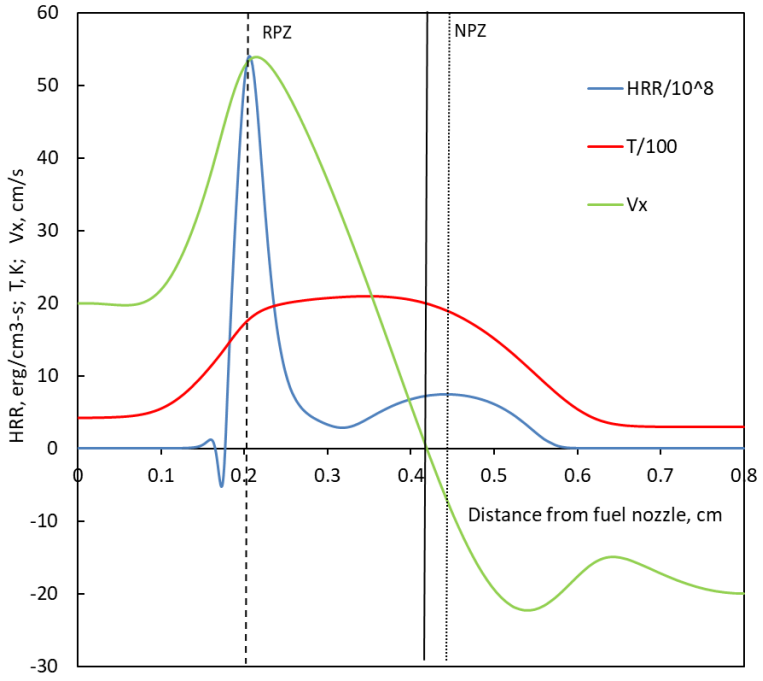

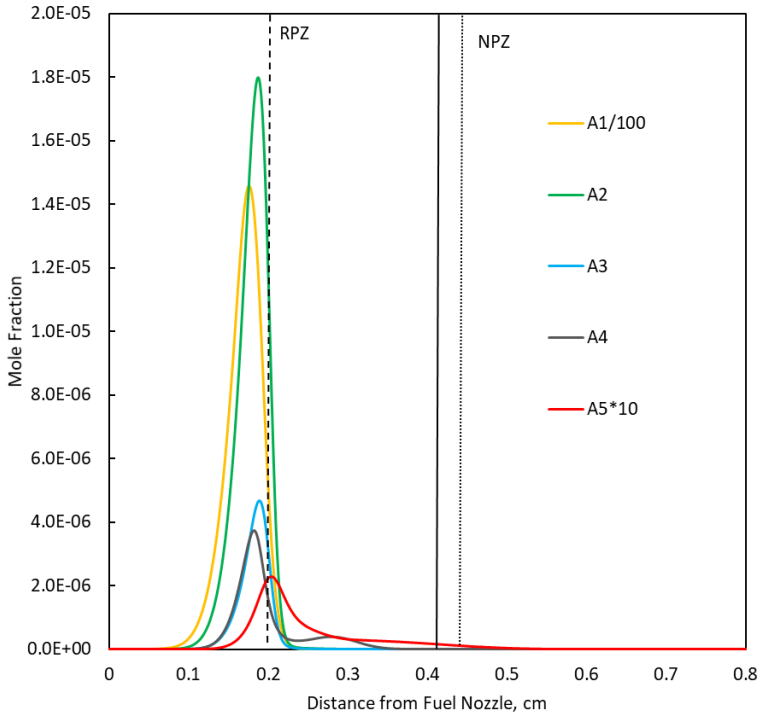

Fig. 24: Flame structure of TPRF70-a partially premixed flame at ϕ = 2. (a) Temperature, HRR, axial velocity, and (b) PAHs mole fractions. Vertical lines represent the locations of rich premixed zone (RPZ), stagnation plane and non-premixed zone (NPZ).

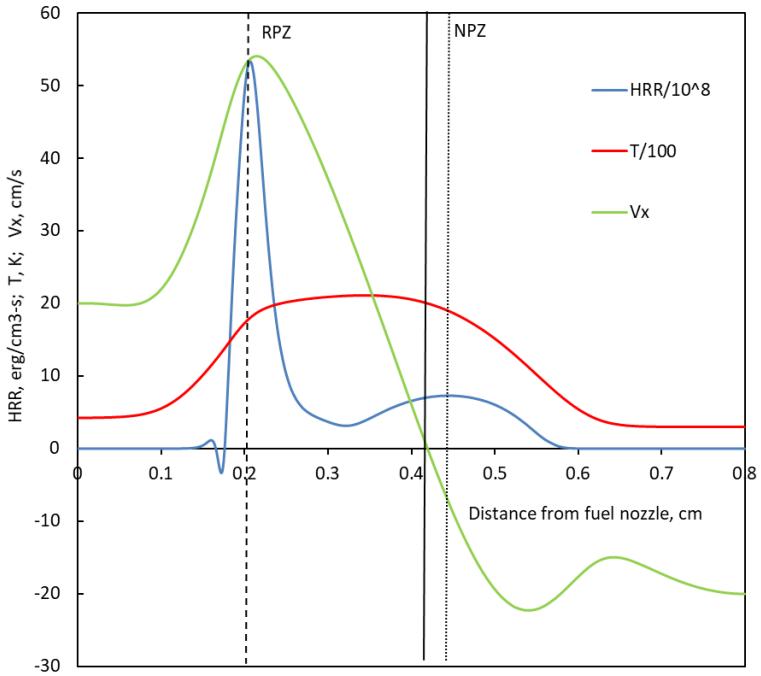

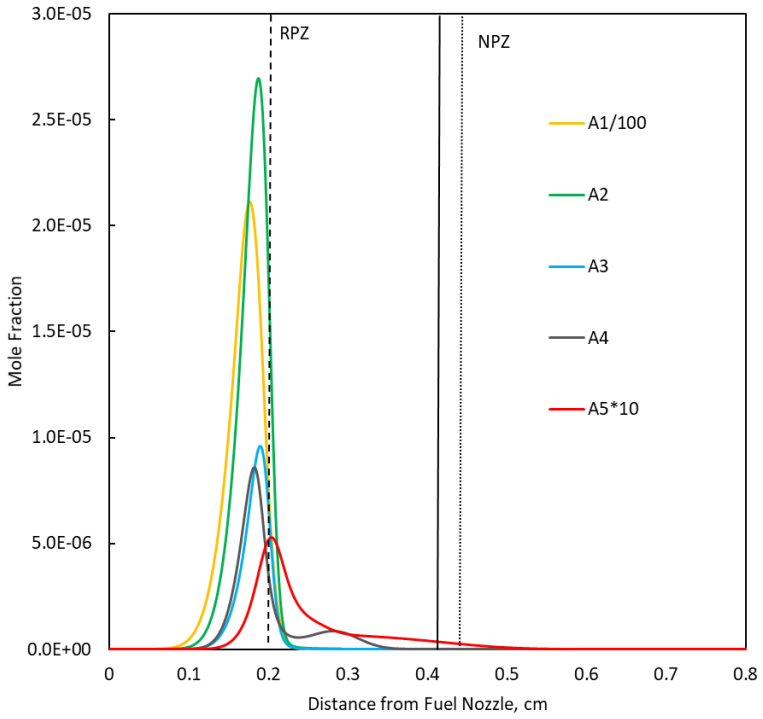

Fig. 25: Flame structure of TPRF70-b partially premixed flame at ϕ = 2. (a) Temperature, HRR, axial velocity, and (b) PAHs mole fractions. Vertical lines represent the locations of rich premixed zone (RPZ), stagnation plane and non-premixed zone (NPZ).

To better comprehend the relative increase in magnitude of PAH species for ternary blends, the peak mole fractions of these PAH species for the three surrogate fuels under consideration are plotted together in a bar chart in Fig 26. Note that in Fig. 26, A1 concentration is scaled down by 100, while the other species indicate their true values. When an aromatic compound, such as toluene, is added into a binary blend made of only paraffinic compounds, the concentrations of PAH species go up significantly, by nearly two orders of magnitude in general. Moreover, the Increase in fuel sensitivity further intensifies the formation of PAH species, as can be observed from the comparison of their concentrations for TPRF70-a and TPRF70-b blends. Thus, it is easy to conclude that higher the fuel sensitivity, greater is the formation of PAH species, and the propensity of the fuel to form soot.

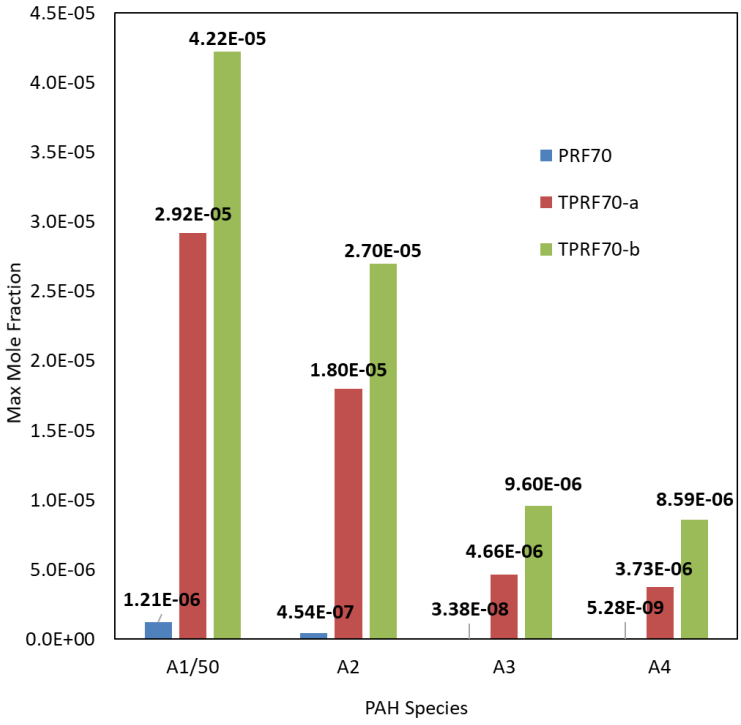

Fig. 26: Peak mole fractions of PAH species (A1-A4) in PRF70, TPRF70-a and TPRF70-b partially premixed flames at ϕ = 2. A1 scaled down by a factor of 50.

Figure 27 presents the important pathways for the formation of benzene (A1) in PRF70 (S=0) and TPRF70-a (S=4) partially premixed flames at ϕ=2. The darker lines represent the major path for benzene formation. As indicated in Fig. 27a, a more important path for benzene formation in the PRF70 flame is from iso-octane. On the other hand, for the ternary blend (Fig. 27b), benzene is mostly formed from toluene due to its ring structure. Since toluene is in the form of phenyl ring structure, it provides the fast route for benzene formation through its reaction with hydrogen radical. The important path for the formation of A1 is through $OC_6H_4CH_3$. In general, this represents the dominant route for benzene formation in flames with ternary fuels (TPRF70-a and TPRF70-b). In the PRF70 flame, the major path includes the formation of propene from iso-octane, which subsequently forms propargyl radicals (C3H3), and then benzene through

the recombination reaction of C3H3. This path is also present in TPRF70-a flames but is significantly less important compared to the toluene path. As further indicated in Fig. 27, for both binary and ternary blends, n-heptane also participates in the formation of propene and propargyl and subsequently benzene. Another route for propargyl formation is through ethylene and acetylene, which are formed from both n-heptane and iso-octane. However, the important observation from Fig. 27 is that due to the ready availability of toluene in ring form, more benzene is formed with ternary blends compared to binary blends.

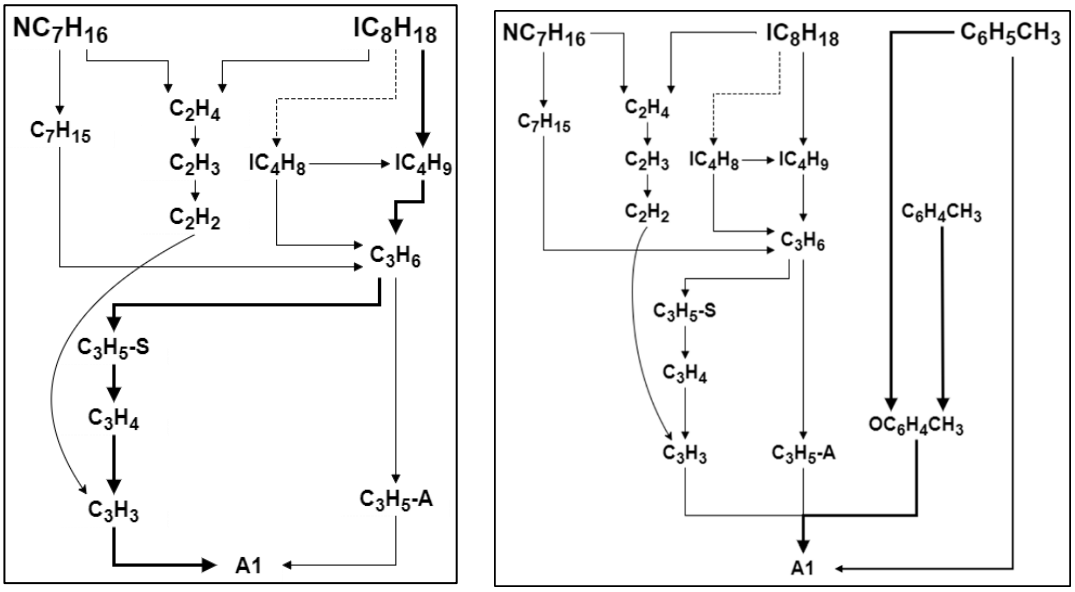

Fig. 27: Key Benzene formation routes in PRF70 (Fig. 27a) and TPRF70-a (Fig. 27b) partially premixed flames at ϕ = 2.

The sensitivity analysis was performed to identify the important reactions participating in production and consumption of PAH species. Figure 28 and 30 present the sensitivity analysis of benzene (A1) and pyrene (A4), respectively for PRF70 (S = 0), TPRF70-a (S = 4) and TPRF70-b (S = 5.7) flames. Moreover, since the soot particle inception models are often based on A1 and A4 concentrations, these species are also important for accurate soot predictions. Figure 28 presents

the sensitivity analysis of A1 (benzene) formation in PRF70, TPRF70-a and TPRF70-b partially premixed flames. And the sensitivity analysis was considered to be done at the location of flame where A1 is highest. Note that the positive sensitivity coefficient implies that the reaction promotes the production of A1 and vice versa. Results indicate that reaction R1302 show high positive sensitivity coefficient implying that this reaction promotes the production of A1 in TPRF70-a and TPRF70-b. Consistent with the results of path analysis, R1302 provide an immediate route for A1 formation in which toluene reacts with hydrogen radical to form benzene. Since PRF70 does not contain toluene or any other aromatic compound, this reaction is not relevant in PRF70.

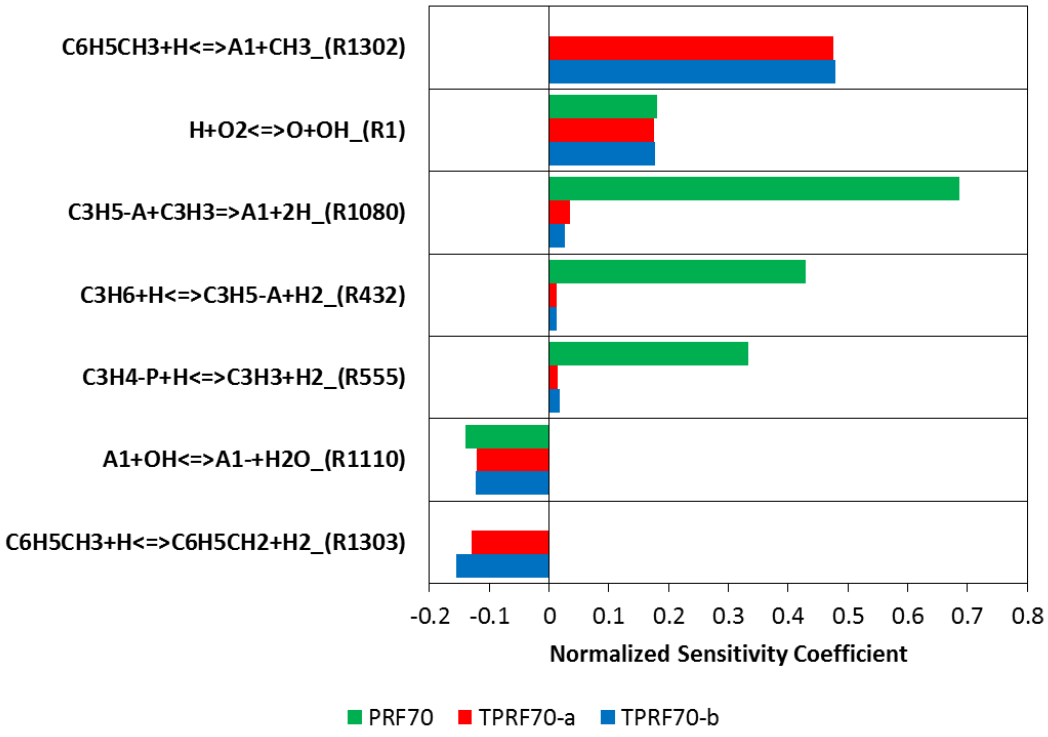

Fig. 28: Sensitivity coefficients of key reactions for benzene (A1) formation in PRF70, TPRF70-a and TPRF70-b partially premixed flames at $\phi = 2$.

For all the three blends the core H2-O2 reaction plays an important role in the production of A1, as reaction R1 (H + O2 = O + OH) show positive sensitive coefficient. But for PRF70 results

indicate that the dominant path for formation A1 is R1080, involving the reaction between propargyl (C3H3) and allyl (C3H5) radicals. Similarly, reaction R432 and R555, has a positive coefficient for binary blend lead to the formation of propargyl (C3H3) and allyl (C3H5) radicals which further participate in reaction R1080. Further reactions responsible for the consumption or oxidation of benzene are R1110 and R1303. Reaction R1110 consume A1 to form A1- to further react to form bigger PAH species. Reaction R1303 involves H-abstraction reaction to form toluene radical, has a negative sensitivity which further reacts to form A4. Reaction R1302 and R1080 are further discussed.

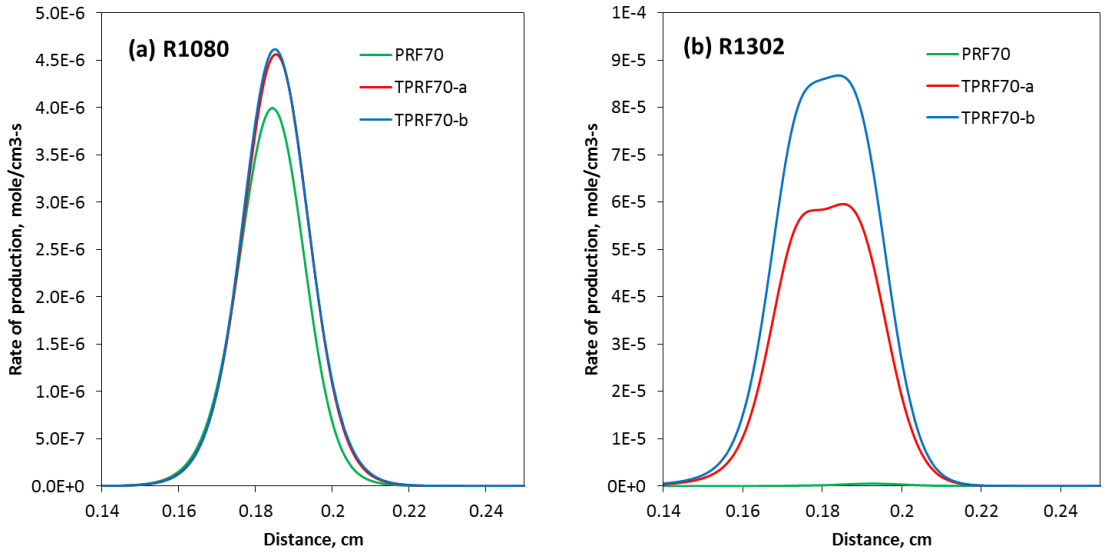

Fig. 29: Rate of production for benzene (A1) through reactions (a) R1080 (left) and (b) R1302 (right) in PRF70, TPRF70-a and TPRF70-b partially premixed flames (ϕ = 2).

Figure 29 present the rate of production of A1 through reaction R1302 in ternary blends flame only and R1080 in all the three blends flame. Although R1080 show higher positive sensitivity coefficient in PR70 flame than ternary blend flame, its rate of production of A1 is higher for TPRF70-a and TPRF70-b as shown in figure 29a. And reaction R1302 show high positive sensitivity coefficient for both TPRF70-a and TPRF70-b, but figure 29b shows that the rate of

production of A1 for TPRF70-b (S = 5.7) is higher. This shows the propensity to form benzene in partially premixed flames is strongly related to the amount of toluene in the fuel blend.

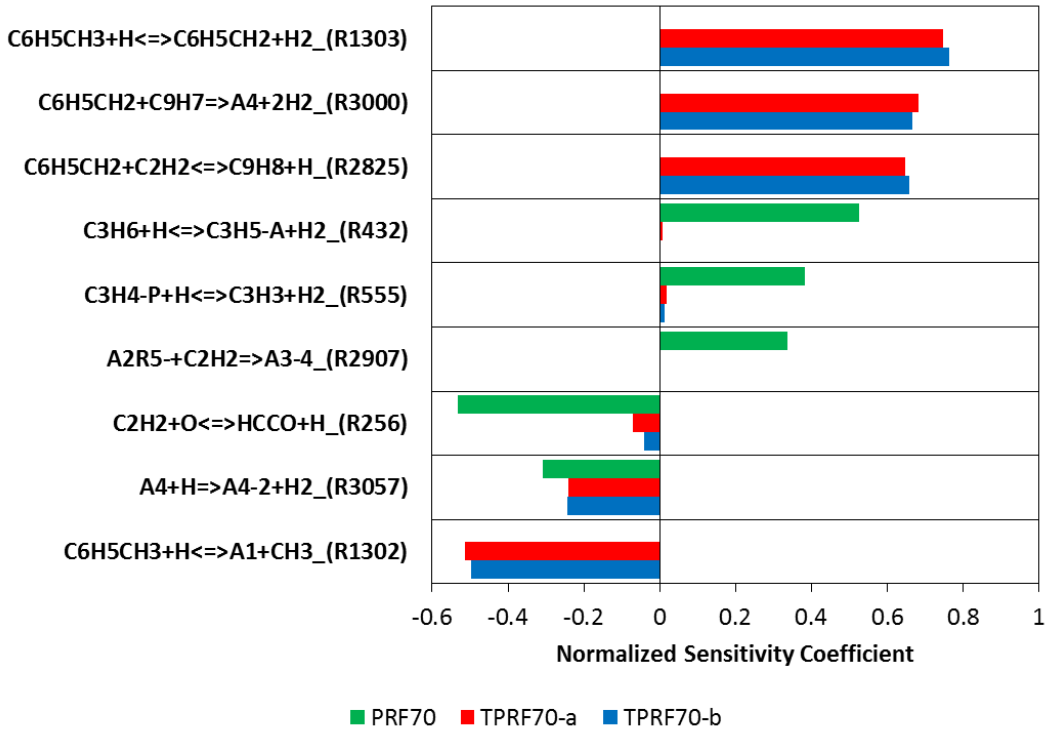

Fig. 30: Sensitivity coefficients of key reactions for pyrene (A4) formation in PRF70, TPRF70-a and TPRF70-b partially premixed flames (ϕ = 2).

Figure 30 presents the results of sensitivity analysis for pyrene (A4) formation in PRF70, TPRF70-a and TPRF70-b partially premixed flames. Again, the sensitivity coefficients were calculated at a location corresponding to the peak A4 mole fraction. Reactions R1303, R2825 and R3000 show high positive sensitivity for A4 formation in TPRF70-a and TPRF70-b flames. All these reactions involve toluene or benzyl radical, which promote the formation of A4. The dominant A4 formation path for TPRF70-a and TPRF7-b is through reaction R3000, in which benzyl radical (C6H5CH2) reacts with indenyl radical (C9H7) to form A4. Reactions R1303 and R2825 form these two radicals and thus promote the formation of A4. R432, R555, and R2907 are important reactions for the formation of A4 in PRF70 flame. As noted earlier, reactions R432 and R555 are

also important in the formation of A1. Reaction R256 has negative sensitivity coefficient since it converts acetylene (C2H2), which is important for the production of PAHs, into an oxygenated product (HCCO). Reaction R3057 shows negative sensitivity coefficient because it H-abstraction process from A4 to form H2, while R1302 is an important reaction for the formation of A1, it reduces the formation of A4 through reaction R1303 and R3000.

5. Conclusion

5.1 **Spray ignition and combustion**

(Previously published as Siddharth Kishor Jain and Suresh K. Aggarwal, Compositional effects on the ignition and combustion of low octane fuels under diesel conditions, *Fuel*, 2018, *220*, 654-670 DOI: 10.1016/j.fuel.2018.02.015)

We have examined the effects of RON and fuel sensitivity (S) on the ignition and combustion behavior of low octane naphtha fuel surrogates in the homogeneous mixtures and diesel sprays. Two binary blends (PRF70 and PRF80) containing iso-octane and n-heptane, and four ternary blends (TPRF70-a, TPRF70-b, TPRF80-a, TPRF80-b), containing iso-octane n-heptane, and toluene were considered. Simulations were performed using a validated reaction mechanism with 109 species and 543 reactions. Important observations are as follow.

(1) For homogeneous mixtures, the fuel sensitivity has a strong influence on ignition at low ($T<850K$) and intermediate ($850K<T<1100K$) temperatures, but relatively small effect at higher ($T>1100K$) temperatures. At low temperatures, the effect of sensitivity is to reduce fuel ignitability, i.e., longer ignition delay. However, as the temperature is increased, the behavior is reversed, indicating shorter ignition delays for blends with higher sensitivity. This implies the existence of a 'transition temperature' at which the fuel ignitability is reversed. Moreover, this transition temperature shifts to higher values as ϕ is increased. Results further indicate that while all the blends exhibit NTC behavior, it becomes less pronounced as the fuel sensitivity is increased.

(2) The sensitivity analysis indicates that the reduced ignitability of ternary blends at low temperatures is primarily due to the consumption of OH by toluene through reaction: C7H8 + OH= C6H5OH + CH3, which acts as a chain termination reaction and slows down the ignition process. Similarly, the increased ignitability of ternary blends at intermediate temperatures is due to three reactions, with R31 that consumes n-heptane and produces n-heptyl radicals, and R39 and R55 that lead to the formation of C6H5CH2O, which subsequently produces OH radicals and thus promotes ignition.

(3) For both homogeneous mixtures and sprays, a two-stage ignition process is observed for all the blends. However, the temperature dependence of the 1st and 2nd stage ignitions is strongly influenced by fuel sensitivity. For homogeneous mixtures at low temperatures (750K), the effect of S is to increase both the 1st stage and 2nd stage ignition times, while at intermediate temperatures (850K), it increases the 1st stage ignition time but decreases the 2nd stage ignition time, and at higher temperatures (1000K), it decreases both the 1st stage and 2nd stage ignition times. While the temperature dependence of two-stage spray ignition is also strongly influenced by fuel sensitivity, there are differences due to spray effects. Compared to homogeneous mixtures, the effective temperature in the spray ignition region is reduced and the effective equivalence ratio may be higher or lower depending upon the vaporization behavior. Consequently, for the range of temperatures investigated, the effect of S is to increase the 1st stage ignition time but decrease the 2nd stage ignition time. Thus, a transition temperature is not observed for spray ignition, although the effect of S becomes less pronounced at higher temperatures.

(4) The ignition kernel structure in sprays is also strongly modified by fuel sensitivity. Since the spray ignitability is enhanced by sensitivity, the ignition kernel in ternary sprays involves richer mixtures, while that in binary (S=0) sprays contains near stoichiometric mixtures, as a consequence, the spray flame structure is modified by sensitivity. While the spray flame in both binary and ternary sprays is characterized by partially premixed combustion involving a lean premixed zone (LPZ), a rich premixed zone (RPZ), and a nonpremixed zone (NPZ), the relative contribution of each zone to total heat release is strongly influenced by sensitivity. It increases the relative contribution of RPZ compared to those of NPZ and RPZ.

(5) The spray flame liftoff length seems to be mainly controlled by ignition behavior. Thus, due to shorter ignition delays, the flame in ternary sprays blends has a smaller liftoff length, i.e., it is located closer to the injector compared to that in binary sprays.

(6) The effect of higher RON is to increase the ignition delay time. Consequently, the ignition kernel involves relatively leaner mixtures, and the flame structure is characterized by increased contributions from LPZ compared to RPZ, and flame liftoff length is increased. Increasing the initial reactor temperature decreases the ignition delay time and thus causes the opposite effect on spray ignition and flame structure.

5.2 **Partially Premixed Counterflow Flame**

We have the examined effects of fuel sensitivity (S) and partial premixing on the PAHs emission of low octane naphtha fuel surrogates in partially premixed counterflow flames. One binary blend (PRF70), containing iso-octane and n-heptane, and two ternary blends (TPRF70-a and TPRF70-b), containing iso-octane, n-heptane, and toluene, were considered. Four different chemical kinetic mechanisms were compared with experimental results to evaluate their predictive capabilities of PAHs emission in opposed jet flame configuration.

1. For validation, the experimental results [21] show that with the increase in iso-octane fraction in ternary blends in counterflow diffusion flames, the PAHs emissions increase monotonically for both 10% and 20% toluene in the blend. The Wang et al [23] and Cai and Pitsch [41] mechanisms show some limitations in predicting this trend. The Wang et al. mechanism predicts increasing emissions initially till 60% iso-octane, but then lower emissions with a further increase in iso-octane fraction. The Cai and Pitsch mechanism predicts PAHs decreasing initially with an increase in the percentage of iso-octane, and then increasing emission. Both the Park et al. [21] and CRECK [42] mechanisms successfully predict the right trend of PAHs emission. But the CRECK mechanism overpredicts the PAHs emissions, while the Park et al. mechanism provides a comparable match with the experimental results.
2. The partially premixed flame results indicate that for all three blends (PRF70, TPRF70-a, and TPRF70-b), the flame structures are similar, with a rich-premixed zone (RPZ) on the fuel side, and a non-premixed zone (NPZ) on the oxidizer side. Most of PAH species are produced close to RPZ for all the three blends and are consumed in the region between RPZ and stagnation plane.

3. With the addition of an aromatic compound, such as toluene, into a binary blend containing only paraffinic compounds, the concentrations of PAH species (A1-A4) go up significantly, by nearly two orders of magnitude in general. Moreover, the increase in fuel sensitivity further intensifies the formation of PAH species. Thus, an important conclusion is that higher the fuel sensitivity, greater is the formation of PAH species, and the propensity of the fuel to form soot.
4. The reaction path and sensitivity analysis for A1 formation in partially premixed flames show that the dominating path for A1 production with ternary blends is through the reaction of toluene with hydrogen radical. In PRF70 flame, the major path includes the formation of propene from iso-octane, which subsequently forms propargyl radicals (C3H3), and then benzene through the recombination reaction of C3H3. This path is also present in TPRF70-a and TPRF70-b flames but is significantly less important compared to the toluene path. Further, the sensitivity analysis for A4 shows that the dominant path for A4 production is through the reaction of benzyl radical (C6H5CH2) and indenyl radical (C9H7).

References

[1] Mobil E. The Outlook for Energy: A View to 2040. Irving, TX: Exxon Mobil. 2012.

[2] Epping K, Aceves S, Bechtold R, Dec JE. The potential of HCCI combustion for high efficiency and low emissions. SAE Technical Paper; 2002-01-1923.

[3] Kalghatgi GT, Risberg P, Ångström HE. Partially pre-mixed auto-ignition of gasoline to attain low smoke and low NOx at high load in a compression ignition engine and comparison with a diesel fuel. SAE Technical Paper; 2007-01-0006.

[4] Subramanian SN, Ciatti S. Low cetane fuels in compression ignition engines to achieve LTC. ASME Paper No. ICEF2011-60014. 2011.

[5] Ciatti S., Subramanian S., An Experimental Investigation of Low-Octane Gasoline in Diesel Engines. ASME J Engineering for Gas Turbines and Power, 2011, 133, 092802-1-11.

[6] Kavuri C., Singh S., Krishnan S. R., Srinivasan K. K., Ciatti S., Computational Analysis of Combustion of High and Low Cetane Fuels in a Compression Ignition Engine. ASME J Engineering for Gas Turbines and Power, 2014, 136, 121506-1-10.

[7] Chang J, Kalghatgi G, Amer A, Viollet Y. Enabling high efficiency direct injection engine with naphtha fuel through partially premixed charge compression ignition combustion. SAE Technical Paper; 2012-01-0677.

[8] Cung K., Rockstroh T., Ciatti S., Cannella W., Goldsborough S., Parametric Study of Ignition and Combustion Characteristics from a Gasoline Compression Ignition Engine Using Two Different Reactivity Fuels. In Proceedings of the ASME 2016 Internal Combustion Engine Fall Conference, ICEF2016-9395.

[9] Yang H, Shuai S, Wang Z, Wang J, Xu H. New premixed compression ignition concept for direct injection IC engines fueled with straight-run naphtha. Energy conversion and management. 2013; 68:161-8.

[10] Zhang Y., Kumar P., Traver M., & Cleary D. (2016). Conventional and Low Temperature Combustion Using Naphtha Fuels in a Multi-Cylinder Heavy-Duty Diesel Engine. SAE International Journal of Engines, 9(2016-01-0764), 1021-1035.

[11] Edgar G. Measurement of knock characteristics of gasoline in terms of a standard fuel1. Industrial & Engineering Chemistry. 1927;19(1):145-6.

[12] Kalghatgi G, Babiker H, Badra J. A simple method to predict knock using toluene, n-heptane and iso-octane blends (TPRF) as gasoline surrogates. SAE International Journal of Engines. 2015;8(2015-01-0757):505-19.

[13] Javed T, Lee C, AlAbbad M, Djebbi K, Beshir M, Badra J, Curran H, Farooq A. Ignition studies of n-heptane/iso-octane/toluene blends. Combustion and Flame. 2016; 171:223-33.

[14] Javed T, Nasir EF, Ahmed A, Badra J, Djebbi K, Beshir M, Ji W, Sarathy SM, Farooq A. Ignition delay measurements of light naphtha: A fully blended low octane fuel. Proceedings of the Combustion Institute. 2017;36(1):315-22.

[15] Knop V, Pera C, Duffour F. Validation of a ternary gasoline surrogate in a CAI engine. Combustion and Flame. 2013;160(10):2067-82.

[16] Rapp VH, Cannella WJ, Chen JY, Dibble RW. Predicting fuel performance for future HCCI engines. Combustion Science and Technology. 2013;185(5):735-48.

[17] Chaos M, Zhao Z, Kazakov A, Gokulakrishnan P, Angioletti M, Dryer FL. A PRF+ toluene surrogate fuel model for simulating gasoline kinetics. In 5th US combustion Meeting 2007 (pp. 25-28).

[18] Gauthier BM, Davidson DF, Hanson RK. Shock tube determination of ignition delay times in full-blend and surrogate fuel mixtures. Combustion and Flame. 2004;139(4):300-11.

[19] Singh E, Badra J, Mehl M, Sarathy SM. Chemical Kinetic Insights into the Octane Number and Octane Sensitivity of Gasoline Surrogate Mixtures. Energy & Fuels. 2017;31(2):1945-60.

[20] Szybist JP, Splitter DA. Pressure and temperature effects on fuels with varying octane sensitivity at high load in SI engines. Combustion and Flame. 2017; 177:49-66.

[21] Park S., Wang Y., Chung S. H., Sarathy S. M. Compositional effects on PAH and soot formation in counterflow diffusion flames of gasoline surrogate fuels. Combustion and Flame, 2017, 178, 46-60.

[22] An Y., Vedharaj S., Vallinayagam R., Dawood A., Masurier J. B., Najafabadi M. I., Johansson B. Effect of Aromatics on Combustion Stratification and Particulate Emissions from Low Octane Gasoline Fuels in PPC and HCCI Mode (No. 2017-24-0086). SAE Technical Paper 2017.

[23] Wang H, Yao M, Yue Z, Jia M, Reitz RD. A reduced toluene reference fuel chemical kinetic mechanism for combustion and polycyclic-aromatic hydrocarbon predictions. Combustion and Flame. 2015;162(6):2390-404.

[24] Mehl M, Pitz WJ, Westbrook CK, Curran HJ. Kinetic modeling of gasoline surrogate components and mixtures under engine conditions. Proceedings of the Combustion Institute. 2011;33(1):193-200.

[25] Reaction Design, CHEMKIN-PRO 15141, Reaction Design, San Diego, 2015.

[26] Engine Combustion Network (ECN). Diesel sprays data search utility. <http://www.sandia.gov/ecn/cvdata/dsearch/frameset.php>

[27] Richards KJ, Senecal PK, Pomraning E. CONVERGE (Version 2.2. 0) Manual, Convergent Science. Inc., Madison, WI. 2014.

[28] Domingo P., Vervisch L. Triple flames and partially premixed combustion in autoignition of non-premixed turbulent mixtures. In Symposium (International) on Combustion. 1996, Vol. 26, No. 1, pp. 233-240

[29] Han Z, Reitz RD. Turbulence modeling of internal combustion engines using RNG κ-ε models. Combustion science and technology. 1995;106(4-6):267-95.

[30] Som S, Aggarwal SK. Effects of primary breakup modeling on spray and combustion characteristics of compression ignition engines. Combustion and Flame. 2010;157(6):1179-93.

[31] Reitz RD, Diwakar R. Structure of high-pressure fuel sprays. SAE Technical Paper; 1987-870598

[32] Patterson MA, Reitz RD. Modeling the effects of fuel spray characteristics on diesel engine combustion and emission. SAE Technical Paper; 1998-980131

[33] Schmidt DP, Rutland CJ. A new droplet collision algorithm. Journal of Computational Physics. 2000;164(1):62-80.

[34] Liu AB, Mather D, Reitz RD. Modeling the Effects of Drop Drag and Breakup on Fuel Sprays. SAE Paper 1993-930072.

[35] Ra Y, Reitz RD. A vaporization model for discrete multi-component fuel sprays. International Journal of Multiphase Flow. 2009;35(2):101-17.

[36] Pomraning E, Richards K, Senecal PK. Modeling turbulent combustion using a RANS model, detailed chemistry, and adaptive mesh refinement. SAE Technical Paper; 2014 -01-1116.

[37] Pickett LM, Bruneaux G, Payri R. Engine combustion network. Sandia National Laboratories, Livermore, CA, http://www. ca. sandia. gov/ecn. 2014.

[38] Som S, D'Errico G, Longman D, Lucchini T. Comparison and standardization of numerical approaches for the prediction of non-reacting and reacting diesel sprays. SAE Technical Paper; 2012-01-1263

[39] Fu X, Aggarwal SK, Fuel unsaturation effects on NOx and PAH formation in spray flames, Fuel. 2015; 160:1-15.

[40] Fieweger K, Blumenthal R, Adomeit G. Self-ignition of SI engine model fuels: a shock tube investigation at high pressure. Combustion and Flame. 1997;109(4):599-619.

[41] Cai L., Pitsch H., Optimized chemical mechanism for combustion of gasoline surrogate fuels, Combustion and flame, 162(5) (2015), 1623-1637.

[42] Bieleveld T., Frassoldati A., Cuoci A., Faravelli A., Ranzi E., Niemann U., Seshadri U. K., Experimental and kinetic modeling study of combustion of gasoline, its surrogates and components in laminar non-premixed flows, Proceedings of the Combustion Institute 32(1) (2009), 493-500.

[43] Aggarwal SK, Awomolo O, Akber K. Ignition characteristics of heptane–hydrogen and heptane–methane fuel blends at elevated pressures. Int J Hydrogen Energy. 2011;36(23):15392-402.

[44] Fu X, Aggarwal SK. Two-stage ignition and NTC phenomenon in diesel engines. Fuel. 2015; 144:188-96.

[45] Sharma S, Aggarwal SK. Effects of Fuel Unsaturation on Transient Ignition and Flame Development in Sprays. Combustion Science and Technology. 2017; doi: 10.1080/00102202.2017.1378649.

[46] Xiao F, Han X, Brezinsky K, Aggarwal S. "Effect of fuel molecular structure and premixing on soot emissions from n-heptane and 1-heptene flames." *Energy & Fuels* 27, no. 10 (2013): 6262-6272.

Appendix

Fuel journal approval:

Please note that, as the author of this Elsevier article, you retain the right to include it in a thesis or dissertation, provided it is not published commercially. Permission is not required, but please ensure that you reference the journal as the original source. For more information on this and on your other retained rights, please visit: https://www.elsevier.com/about/our-business/policies/copyright#Author-rights

VITA

NAME: Siddharth Kishor Jain

EDUCATION: B. E. Mechanical Engineering, University of Mumbai, Mumbai, India. 2015

M. S. Mechanical Engineering, University of Illinois at Chicago, Chicago, Illinois, 2017

EXPERIENCE: Performance and Emissions Engineer, Daimler Trucks North America, Detroit, MI (Present)

Intern – Medium Duty Performance Engineer, Daimler Trucks North America, Detroit, MI (2018)